Periodic ground state for the charged massive Schwinger model

S. Nagy[1], J. Polonyi[2,3], and K. Sailer[1]
[1] *Department for Theoretical Physics, University of Debrecen, Debrecen, Hungary*
[2] *Institute for Theoretical Physics, Louis Pasteur University, Strasbourg, France*
[3] *Department of Atomic Physics, Lorand Eötvös University, Budapest, Hungary*
(February 1, 2008)

It is shown that the charged massive Schwinger model supports a periodic vacuum structure for arbitrary charge density, similar to the common crystalline layout known in solid state physics. The dynamical origin of the inhomogeneity is identified in the framework of the bozonized model and in terms of the original fermionic variables.

12.20.Ds

I. INTRODUCTION

An important feature of Quantum Field Theories is the formal separation of the "active" and "spectator" degrees of freedom. In fact, the conventional contributions to the perturbation series of a Green function, represented by Feynman graphs, involve more and more actively participating particles as the order of the expansion is increased and the ground state with its infinitely many real or virtual particles remains formally hidden. This scheme is really efficient only if the vacuum is "empty" which is usually realized by the adiabatic turning on and off the interactions as the time evolves. But serious complications arise in this scheme when the vacuum is "non-empty", i.e. contains a significant number of particles. When the constituents of the vacuum form a rigid system then the vacuum is called solid and space-symmetries are violated. When the constituents are not localized then the vacuum can be considered as liquid.

When the fluctuations are sufficiently small then the saddle point expansion can be used to turn this qualitative picture into a systematical description. The "non-empty" vacuum consists of a condensate in this scheme. What is the momentum of the condensed particles? In case of vanishing momentum the vacuum is homogeneous and the dynamics of the excitations can be described in a straightforward manner. But it may happen that the vacuum is made up by particles of non-vanishing momentum in which case the saddle point is inhomogeneous and breaks the space-time symmetries. Depending on the 'inertia' of the saddle point the zero modes arising from this formal symmetry breaking are either integrated over (liquid) or kept at a fixed value (solid).

A few examples for liquids are the following. The short range correlations of the vacuum in Yang-Mills models correspond to a liquid of localized tree-level saddle points, instantons [1]. The one-loop effective action indicates the presence of other condensates [2] which must be inhomogeneous in order to preserve the external and internal symmetries. The mixed phase at first order phase transitions and the corresponding Maxwell-cut results from the soft modes which are generated by the inhomogeneous saddle points of the Kadanoff-Wilson blocking procedure in renormalizing the action [3]. The metallic lattice is the best known example of solids, and similar, periodically modulated ground state belongs to the Wigner lattice of dilute electron gas [4] or the charge density wave phase in solids [5].

Our current understanding of such vacua is severely limited due to the strong interactions or correlations between the "active" and the "spectator" particles. This is easy to understand in the framework of the saddle point expansion. The soft zero modes of the inhomogeneous saddle points in a liquid are easy to excite and they usually lead to serious IR divergences in the semiclassical expansion. There may not be soft modes present in the ground state of a solid but momenta borrowed from the inhomogeneous condensate generate nonperturbative phenomena such as the opening of gaps. In addition to the strong coupling between the "active" and "spectator" degrees of freedom the dynamical origin of the condensation and the explicit construction of the ground state from first principles represent a so far unmatched challenge in both cases. We believe that the treatment of the soft modes is a more serious and difficult problem than those of the momentum nonconserving processes. The goal of the present work is to trace the origin of the periodically modulated vacuum in one of the simplest interactive theory, Quantum Electrodynamics in 1+1 dimensions, the Schwinger model [6].

Which part of the (effective) action is responsible of the inhomogeneity of the vacuum? The inhomogeneity suggests the presence of strongly distance-dependent interactions in the system and it is natural to expect that such interactions arise from the higher derivative terms in the action rather than from the ultralocal potential energy. Such a relation between the presence of higher order derivative terms with sufficiently strong coefficients in the action and

the inhomogeneity of the vacuum has already been confirmed in a number of cases [7]. What was left open by these works is the dynamical origin of the higher order derivative terms in the effective action which drive the condensation at nonvanishing momentum. The higher order derivative terms which are supposed to be responsible for an eventual inhomogeneity in QED are to be sought in the effective theory for the photons or for the density. The simplifications which occur when we constrain ourselves into 1+1 dimensions allow us to use simple but powerful analytical and numerical methods, such as bosonization and the variational approach, to explore these effective theories in a nonperturbative manner. The main result of this work is that the vacuum of the massive Schwinger model in the presence of nonvanishing total electric charge is periodically modulated. It is reassuring that both the bosonization and the variational approach yield the same conclusion. The bosonization allows to identify a mechanism, more involved as anticipated in the works [7], as the driving force in forming the periodically modulated vacuum. The inhomogeneity arises from the competition of an unusual piece of the kinetic energy which contains the first power of the space derivative, the boundary conditions and the periodic part of the potential energy. The periodicity of the vacuum field configuration in space originates from the periodicity of a term in the potential energy in the field variable.

The Schwinger model has already been extensively investigated. What will be important from the point of view of the present work is that the confinement of the electric charge has been established [8–11] and simple analytic considerations hint that the vacuum with nonvanishing background charge is inhomogeneous [11].

It is worth mentioning that a non-trivial vacuum structure appears in QCD_4 as well at high fermion densities within the large N_c expansion [12]. This result motivated the search for periodic structure in two-dimensional field theoretical models where the investigation can be carried out without approximations. It was found that the Gross-Neveu and the 't Hooft models exhibit periodic baryon density [13], and the multiflavor Schwinger model and QCD_2 also shows up periodic ground state [14].

The resemblance of the Schwinger model to a one-dimensional electron system may one also lead to the idea of the existence of a periodic ground state. Some compounds can have such atomic structure that they exhibit one-dimensional metallic properties and show periodic structure [15]. An analogue of the Wigner crystal appears in a one-dimensional spin system with short range, nearest neighbour interaction [16], and a one-dimensional electron gas with a long range $U(r) \sim 1/r$ type Coulomb potential also exhibits periodic ground state [17]. Another indication of the inhomogeneous vacuum structure in one spatial dimension comes from the non-relativistic Peierls mechanism [18].

The massless Schwinger model is exactly solvable [19] and the explicit computation of the fermion determinant leads to an effective theory with massive photons and confinement [9]. When the vacuum polarization effects are neglected then the electric flux conservation induces a flux tube between an electron-positron pair in the absence of other charges. The resulting linear potential, the hard confinement mechanism, renders the positronium confined. Let us now allow the vacuum polarization to be present and try to separate a member of the positronium, that of the meson of the Schwinger model. The electric flux tube breaks up due to electron-positron pair creation when the energy of the stretched flux tube is sufficiently large and the members of the newly created pair bind to those of the original pair. This is the soft confinement mechanism and one ends up with more neutral mesons again in this manner. The linear potential between the electron-positron pair becomes saturated by virtual pair creations. The potential between a pair of static test charges can easily be obtained in the presence of vacuum polarization [9] and it shows that the total screening, the soft confinement mechanism, occurs for arbitrary value of the charge.

The massive Schwinger model is not exactly solvable and the potential between a pair of test charges is periodic function of the charge with period length given by the elementary charge e and is saturated for integer multiples of e only [9]. The mass gap prevents the vacuum to screen out non-integer multiples of the elementary charge. Notice that the massless model is singular in the sense that arbitrarily small mass is enough to prevent the screening of non-integer charges at sufficiently large distances. At the end any charge is confined in the massive model as well but the integer or non-integer charges are confined by the soft or hard mechanisms, respectively.

Excitations above a fermionic vacuum with well-defined particle number are always consisted of particle-hole pairs and are therefore of bosonic nature. It is the special feature of the 1+1 dimensional world that the effective theory for these bosonic excitations is local. The local effective theory resulting from the bosonization of the massive Thirring model is the sine-Gordon model [20]. These bosonization rules are widely used for the investigation of the Schwinger model [10,11,21–23]. The massless case yields a free scalar theory and the massive theory leads to the massive sine-Gordon model [24]. The massive Schwinger model was also investigated by bosonization technique [25] and by functional methods [26] at non-vanishing chemical potential μ and temperature T. The existence of a periodic chiral condensate with the wavenumber of 2μ has been established for arbitrary temperature, too.

Arguments were given in the framework of the tree-level solution of the bosonized model [11] that the massive Schwinger model exhibits a periodic ground state in the presence of a static, homogeneous background charge density. A more systematic investigation of the inhomogeneity of the vacuum of the massive Schwinger model in the presence of homogeneous external charge density, $\rho_{\rm ext}$, is presented in this paper. We attack the problem from two different directions. First by minimizing the tree-level expression of the energy functional in the bosonized form of the model

and after that by minimizing the energy with respect to the parameters of a static, periodic background electric field in the fermionic form of the theory and by retaining the quantum fluctuations of the photon field up to the two-loop order. The results obtained by both approaches are in qualitative agreement. Namely, the ground state exhibits periodically modulated charge density with decreasing amplitude for increasing $\rho_{\rm ext}$. For large $\rho_{\rm ext}$ numerical calculations failed to be conclusive regarding the true energy minimum. Analytic considerations were used in this density regime with the result that the vacuum remains periodic for arbitrarily large values of $\rho_{\rm ext}$.

The paper is organized as follows. Section II contains the study of the tree-level bosonized theory in the presence of the homogeneous external charge density $\rho_{\rm ext}$. The minimum of the energy functional of the model is found by numerical minimization of the classical vacuum energy. For large values of $\rho_{\rm ext}$ when the result is more unstable with respect to numerical errors the stability of the periodic vacuum has been shown analytically, by expanding the tree-level energy in powers of the amplitude of charge density wave in the vacuum.

The fermionic investigations are presented in Section III. Since integer charges are screened and do not leave behind long range photon field [11] the perturbation expansion in e is reliable by using the original fermionic and photonic degrees of freedom. We follow a variational strategy and minimize the energy of the vacuum as the function of the induced photon field in the vacuum. The fermionic degrees of freedom are integrated out in the presence of a static, sinusoidal electric field and the quantum fluctuations of the photon field are taken into account up to two-loop diagrams for the energy. The external charge density $\rho_{\rm ext}$ is introduced indirectly via a fermionic chemical potential μ. The energy of the vacuum is finally minimized with respect to the amplitude and the wavelength of the static periodic background electric field. The numerical minimization procedure finds the periodic ground state energetically favorable as compared to the homogeneous one below certain value of $\rho_{\rm ext}$. The problem of the high density regime is of the same origin as in the bosonized study, namely the smallness of the amplitude of the induced photon field in the vacuum. An analytic calculation in the framework of the perturbation expansion in the amplitude of the induced photon field predicts a periodic ground state even in this density region.

Finally, the conclusion is drawn up in Sect. IV. Appendices A and B present briefly the numerical solutions of the Dirac equation in periodic background potential and the band structure of the fermionic spectrum, respectively. Explicit expressions for the Feynman diagrams for the energy and charge densities up to the two-loop order are given in Appendix C, and the details of the numerical search for the energy minimum are given.

II. MINIMIZATION OF THE ENERGY IN THE BOSONIZED MODEL

This section contains the tree-level determination of the vacuum structure of the bosonized model.

A. Hamiltonian

The Lagrangean of the massive Schwinger model is given as

$$\mathcal{L} = -\frac{1}{4}F_{\mu\nu}F^{\mu\nu} + \bar{\psi}\gamma^{\mu}(\partial_{\mu} - \mathrm{i}eA_{\mu})\psi - m\bar{\psi}\psi, \tag{1}$$

where $F_{\mu\nu} = \partial_{\mu}A_{\nu} - \partial_{\nu}A_{\mu}$, m and e are the bare rest mass of the electron and the bare coupling constant, respectively. The bosonization rules are [11]:

$$\begin{aligned} :\bar{\psi}\psi: \;&\to\; -cmM\cos(2\sqrt{\pi}\phi), \qquad & :\bar{\psi}\gamma_5\psi: \;&\to\; -cmM\sin(2\sqrt{\pi}\phi), \\ j_{\mu} =: \bar{\psi}\gamma_{\mu}\psi: \;&\to\; \tfrac{1}{\sqrt{\pi}}\varepsilon_{\mu\nu}\partial^{\nu}\phi, & :\bar{\psi}\mathrm{i}\partial\!\!\!/\psi: \;&\to\; \frac{1}{2}N_m(\partial_{\mu}\phi)^2, \end{aligned} \tag{2}$$

where N_m denotes normal ordering with respect to the fermion mass m, $c = \exp(\gamma)/2\pi$ with the Euler constant γ, and $M = e/\sqrt{\pi}$ the 'meson' mass. It is believed that the presence of a non-vanishing background charge density does not affect these transformation rules [25]. The Hamiltonian of the system in Coulomb gauge is given by

$$\mathcal{H} = \int_x \bar{\psi}_x(\mathrm{i}\gamma_1\partial_1 + m)\psi_x - \frac{e^2}{4}\int_{x,y} j_{0,x}|x-y|j_{0,y}, \tag{3}$$

with $\int_x = \int_0^T dx^0 \int_{-L}^{L} dx^1$. According to the bosonization rules this Hamiltonian is equivalent to those of the massive sine-Gordon model,

$$\mathcal{H}[\Pi,\phi] = N_m \int_x \left[\frac{1}{2}\Pi_x^2 + \frac{1}{2}(\partial_1\phi_x)^2 + \frac{1}{2}M^2\phi_x^2 - cmM\cos(2\sqrt{\pi}\phi_x)\right] \tag{4}$$

where Π_x denotes the momentum variable canonically conjugated to ϕ_x.

Our purpose is to determine the vacuum of the massive Schwinger model in the presence of an external static particle density $\rho_{\mathrm{ext}\ x}$ which is added to the density $j_{0,x}$ in Eq. (3),

$$\mathcal{H}_{\mathrm{ext}} = \int_x \bar{\psi}_x(\mathrm{i}\gamma_1\partial_1 + m)\psi_x - \frac{e^2}{4}\int_{x,y}(j_{0,x} + \rho_{\mathrm{ext}\ x})|x-y|(j_{0,y} + \rho_{\mathrm{ext}\ y}). \tag{5}$$

The external charge is represented by the external field $\phi_{\mathrm{ext}\ x}$ in the bosonized Hamiltonian (4) as

$$\mathcal{H}_{\mathrm{ext}}[\Pi,\phi] = N_m \int_x \left[\frac{1}{2}\Pi_x^2 + \frac{1}{2}(\partial_1\phi_x)^2 + \frac{1}{2}M^2(\phi_x + \phi_{\mathrm{ext}\ x})^2 - cmM\cos(2\sqrt{\pi}\phi_x)\right] \tag{6}$$

where

$$\rho_{\mathrm{ext}\ x} = \frac{1}{\sqrt{\pi}}\partial_1\phi_{\mathrm{ext}\ x}. \tag{7}$$

The external particle density is assumed to be static and constant in the interval $x^1 = z \in [-L, L]$ and vanishing elsewhere, therefore we write $\phi_{\mathrm{ext}\ x} = bz$ when $|z| \leq L$ and $\phi_{\mathrm{ext}\ x} = 0$ elsewhere for any $x^0 = t$. It is advantegous to introduce the field variable

$$\tilde{\phi}_z = \phi_z + bz \tag{8}$$

which allows us to write the total particle density as

$$\rho_x = \frac{1}{\sqrt{\pi}}\partial_1\tilde{\phi}_x. \tag{9}$$

The tree-level vacuum can be constructed by minimizing the Hamiltonian (4) as the functional of the static field configuration ϕ_x with $\Pi_x = 0$. The minimum is reached at $\phi_{\mathrm{gr}\ x} = \langle 0|\phi_x|0\rangle$ and the value of the Hamiltonian at this field configuration, $E(b) = \mathcal{H}_{\mathrm{ext}}[0,\phi_{\mathrm{gr}}]$, can be identified by the tree-level vacuum energy. Lattice regularization of the Hamiltonian for static field,

$$\mathcal{H}_{\mathrm{ext}}[0,\phi] = \int_z \left[\frac{1}{2}(\partial_1\phi_z)^2 + \frac{e^2}{2\pi}(\phi_z + bz)^2 - \frac{cme}{\sqrt{\pi}}\cos(2\sqrt{\pi}\phi_z)\right], \tag{10}$$

yields

$$a\mathcal{H}_L[0,\phi] = \frac{1}{2}\sum_{n=0}^{N}(\phi_{n+1} - \phi_n)^2 + \frac{e_L^2}{2\pi}\sum_{n=0}^{N}(\phi_n + bz_n)^2 - \frac{cm_Le_L}{\sqrt{\pi}}\sum_{n=0}^{N}\cos(2\sqrt{\pi}\phi_n), \tag{11}$$

where a stands for the lattice spacing, $e_L = ea$, $m_L = ma$, $z_n = z_0 + na$, $a = 2L/(N+1)$, $z_0 = -L$, $z_{N+1} = L$ and $\phi_n = \phi_{z_n}$. The boundary conditions

$$\phi_0 = \phi_{N+1} = 0 \tag{12}$$

have been used in order to restrict the computation into the sector with vanishing induced charge.

In order to understand the origin of the periodic structure of the vacuum we rewrite the static Hamiltonian (11) in terms of the shifted variable $\tilde{\phi}$ as

$$a\tilde{\mathcal{H}}_L[0,\tilde{\phi}] = \frac{1}{2}\sum_{n=0}^{N}(\tilde{\phi}_{n+1} - \tilde{\phi}_n - \sqrt{\pi}\rho_{\mathrm{ext}\ L})^2 + \frac{e_L^2}{2\pi}\sum_{n=0}^{N}\tilde{\phi}_n^2 - \frac{cm_Le_L}{\sqrt{\pi}}\sum_{n=0}^{N}\cos(2\sqrt{\pi}(\tilde{\phi}_n - bz)), \tag{13}$$

where $\rho_{\mathrm{ext}\ L} = a\rho_{\mathrm{ext}} = ab/\sqrt{\pi}$ denotes the amount of external particles distributed between two consecutive lattice sites. This expression reveals a competition in forming the vacuum, taking place between the kinetic and the potential energies, the first and the remaining terms on the right hand side of Eq. (13). Let us first ignore for simplicity the quadratic mass term and the shift $-bz$ in the argument of the cosine function on the right hand side, a simplification

which yields the Hamiltonian of the Frenkel-Kontorova model [27]. The tree-level vacuum of this model produces infinitely many commensurate-incommensurate transitions and displays a rather involved phase structure with the devil-staircase feature due to the competition between two dimensionless parameters [28]. In fact, the kinetic energy prefers

$$\tilde{\phi}_n = \text{const.} + n\sqrt{\pi}\rho_{\text{ext }L} \tag{14}$$

and the potential energy is minimal for $\tilde{\phi}_n = j\sqrt{\pi}$ (with n and j integers) and the vacuum is trivial, i.e. a linear function of the coordinate, for integer $\rho_{\text{ext }L}$ only. The vacuum of the complete Hamiltonian (13) is always the result of a compromise between the kinetic energy with the preference expressed by Eq. (14) and the potential energy which prefers $\tilde{\phi} = 0$ and $\tilde{\phi}_n = \sqrt{\pi}(j - n\rho_{\text{ext }L})$. The competition between the kinetic and the potential energy is never trivial due to the quadratic mass term but is at least simplified when $\rho_{\text{ext }L}$ is integer. For sufficiently small lattice spacing $\rho_{\text{ext }L} < 1$ each energy expression on the right hand side of Eq. (13) enters in the competition for the vacuum.

Such an involved vacuum structure is characteristic of the tree-level solution in lattice regularization only. The quantum fluctuations should smear most of the commensurate-incommensurate transitions out. A similarly smeared behaviour is what one finds when the cutoff is ignored in the tree-level sector, i.e. when the minimum energy configuration is searched in the naive, classical continuum limit of Eq. (13),

$$\tilde{\mathcal{H}}_{\text{ext}}[0,\tilde{\phi}] = \int_z \left[\frac{1}{2}(\partial_1\tilde{\phi}_z - \sqrt{\pi}\rho_{\text{ext}})^2 + \frac{e^2}{2\pi}\tilde{\phi}_z^2 - \frac{cme}{\sqrt{\pi}}\cos(2\sqrt{\pi}(\tilde{\phi}_z - \sqrt{\pi}\rho_{\text{ext}}z))\right], \tag{15}$$

subject of the boundary conditions $\tilde{\phi}_{-L} = 0$, $\tilde{\phi}_L = 2\sqrt{\pi}L\rho_{\text{ext}}$. In the Frenkel-Kontorova limit when the mass term and the z-dependence in the argument of the cosine function are ignored then ϕ_z develops oscillatory structure in the vacuum which changes smoothly with the parameters of the model. In fact, the kinetic energy prefers to distribute the total change $\tilde{\phi}_L - \tilde{\phi}_{-L} = 2\sqrt{\pi}L\rho_{\text{ext}}$ in a linear manner but the potential energy introduces a periodic modulation. The period length can be determined by noting that $\tilde{\phi}$ should change by $\sqrt{\pi}$ within a period. Such a simple argument gives the period length $\ell_0 = 1/\rho_{ext}$ for small me. The fermions correspond to kinks of the sine-Gordon model according to the bosonization therefore it is not surprising to find that there is just one particle per period in such a vacuum state. The z-dependent shift in the cosine function takes out the driving linear term from $\tilde{\phi}$ but tends to generate periodic oscillations with the same period length.

Notice that the source of the inhomogeneity of the vacuum is an unusual, $\mathcal{O}(\partial_1)$, gradient term in the kinetic energy. This contribution to the energy, together with the boundary conditions and the periodic potential energy form the periodic modulation in the vacuum. Furthermore the space inversion symmetry is broken explicitly by the $\mathcal{O}(\partial_1)$ term and the boundary conditions. It is interesting to compare this situation with those encountered in earlier studies [7] where the dispersion relation of the form

$$\epsilon(p) = C_6 p^6 + C_4 p^4 + \frac{p^2}{2} + C_0 \tag{16}$$

was used with $C_6, -C_4 > 0$ with non-periodic potential energy and the tree-level vacuum is expected to be periodic if there is a region in the momentum space where $\epsilon(p) < 0$. The space-time inhomogeneities are therefore generated by the competition of terms with different orders of the gradient only and the space inversion symmetry is broken spontaneously.

B. Numerical results

The energy minimum was searched by the conjugate gradient method which started from a number of initial conditions for ϕ_{z_i} and the field configurations corresponding to the lowest energy only have been singled retained. The charge densities were then calculated according to Eq. (9). We used $L = 16\pi$, $N = 800$, $m = 0.5; 2; 5$ and $b \in [0.3; 7]$ in the numerical studies.

The minimum of the expression (10) was found at $\phi_z = 0$ for vanishing external charge density, i.e. for $b = 0$. The increase of b gave two distinct regions, separated by a size-dependent point $b = b_L$.

$\underline{b < b_L}$: For b close to zero one expects that ϕ_z is small and the sinusoidal potential in the equation of motion,

$$\partial_1\phi_z = \frac{e^2}{\pi}(\phi_z + bz) + 2cme\sin(2\sqrt{\pi}\phi_z), \tag{17}$$

can well be approximated by the first term of its Taylor series

$$\partial_1 \phi_z \approx \frac{e^2}{\pi}(\phi_z + bz) + 4cme\sqrt{\pi}\phi_z. \tag{18}$$

Such a linearized equation of motion together with the boundary conditions (12) yields

$$\phi_z = b_s L \frac{\sinh(\kappa z)}{\sinh(\kappa L)} - b_s z, \quad \kappa = \sqrt{\frac{e^2}{\pi} + 4cme\sqrt{\pi}}, \quad b_s = b\frac{e^2}{\kappa^2 \pi}. \tag{19}$$

This solution, shown in Fig. 1, contains three spatial regions in the interval $[-L, L]$ and in the longest, central region ϕ_z is linearly decreasing function with the slope $-b_s$. The analytic results for the slope are in very good agreement with those obtained numerically. The linear decrease of ϕ_z in the central region describes the partial screening of the external charge density. In the two other regions, close to the boundaries at $-L$ and L, $|\phi_z|$ approaches abruptly zero. For every choice of L a critical b_L value was found where the linear approximation fails to work and the higher-order terms of the sine function are needed in the equation of motion (17). It was found that the slope b_s reaches b at this point. The L-dependence is $b_L \approx L^{-1.41}$ according to Fig. 2, therefore $b_L \to 0$ and this type of solutions disappears in the thermodynamic limit.

$\underline{b_L < b}$: The increase of b_s to b indicates the complete screening of the external charge density in the central region. Furthermore the numerical solution, depicted in Fig. 3, reveals an additional periodic structure in ϕ_z, $\tilde{\phi}_z$ is a periodic function of wavelength ℓ, $\tilde{\phi}_z = \tilde{\phi}_{z+\ell}$. The wavelength ℓ and the amplitude A of $\tilde{\phi}_z$ were defined numerically as the distance of the neighbouring zeros of $\tilde{\phi}_z$ and the arithmetic average of the magnitude $|\tilde{\phi}_z|$ at the extrema of the periodic component, respectively. Both ℓ and A decrease with increasing b in this region as shown in Figs. 4 and 5. This feature opens the possibility of applying the perturbation expansion in the amplitude A of the induced periodic field in the vacuum in the limit of asymptotically large charge densities, $\rho \to \infty$. Based on Fig. 3 the periodic part of the scalar field is approximated by

$$\tilde{\phi}_z = A \sin\left(\frac{2\pi}{\ell} z\right). \tag{20}$$

By inserting this expression into Eq. (10) one finds the energy density

$$\mathcal{E}(A, b) \equiv \frac{E(b)}{2L} = \frac{A^2\pi^2}{\ell^2} + \frac{\pi}{2\ell^2} + \frac{e^2A^2}{4\pi} - \frac{cme}{\pi^{1/2}} J_1(2\sqrt{\pi}A), \tag{21}$$

where $J_1(x)$ is the Bessel function of the first kind. Fig. 4 shows that the amplitude A decreases with increasing charge density. Therefore it is sufficient to consider the expression on the right hand side of Eq. (21) only up to the order $\mathcal{O}(A^2)$ for large $\rho \to \infty$. Due to the relation

$$J_1(x) \approx \frac{x}{2} + \mathcal{O}(x^3) \tag{22}$$

valid for small x the energy density takes the form

$$\mathcal{E}(A, b) = \frac{b^2}{2} + \frac{A^2}{4}\left(4\pi b^2 + \frac{e^2}{\pi}\right) - cmeA \tag{23}$$

having a non-trivial minimum at

$$A = \frac{2cme}{4\pi b^2 + \frac{e^2}{\pi}} > 0 \tag{24}$$

where the Casimir energy is negative,

$$\mathcal{E}(A, b) - \mathcal{E}(A = 0, b) = -\frac{(cme)^2}{4\pi b^2 + \frac{e^2}{\pi}} < 0. \tag{25}$$

Thus one concludes that the ground state of the massive Schwinger model is periodic for large external charge densities. It is shown in Fig. 4 that the analytic result of Eq. (24) is in good agreement with the numerical one for the charge-dependence of the amplitude A.

The relation $\ell = 1/\rho_{\text{ext}}$ displayed by Fig. 5 reflects the fact that charges which are integer multiples of e are completely screened. In fact, as argued in Ref. [11], the introduction of the charges $\pm e$ at the boundaries corresponds

to the shift $z \to z + \delta z$ with $|\delta z| = \sqrt{\pi}/b$. This is a symmetry of the vacuum if $\tilde{\phi}_z$ has the length of period $\ell = |\delta z|/\nu$ where ν is integer. According to the numerical results $\nu = 1$ at the energy minimum. Similar periodic structure is found in Wigner crystals of itinerant electrons, in certain spin systems [16] and in the charge density wave states. The periodicity usually gives way to homogeneity when the external charge density is increased because the overlap integrals between the neighbouring lattice sites increase. This is not what happens in the massive Schwinger model, where the simple, leading order perturbation expansion given above shows that the ground state keeps its periodicity for arbitrarily large charge densities.

Our conclusion is that in the tree-level approximation of the bosonized theory the massive Schwinger model has a single periodic phase in the thermodynamic limit and the homogeneous external charge density is neutralized in average by a periodic, induced charge density. Integer charges are completely screened as argued in [11].

III. VARIATIONAL MINIMIZATION OF THE ENERGY FOR QED$_{1+1}$

Let us consider now the massive Schwinger model in terms of the original fermionic degrees of freedom and subject to periodic boundary conditions at the endpoints of a finite spatial interval. The finite charge density is now introduced by the chemical potential μ. The system of electrons is easier to polarize than the 'empty' vacuum and accordingly there is no gap in the free electron excitation spectrum for $\mu > m$. The photon polarization tensor is non-vanishing at the Fermi level therefore the Debye screening renders the photon propagator short ranged and the Coulomb potential vanishing for large separation [29]. Our computation performed in this formalism supports the results obtained in the bosonized theory, namely that even an arbitrarily weak interaction among the electrons is sufficient to form a periodic ground state. The dynamical origin of the modulated ground state is the opening of a gap around the Fermi level.

We are confronted by two complications in describing the vacuum. First, the confinement of charge renders the fermionic excitation spectrum non-physical and ill-defined. As discussed above in the framework of the bosonized theory integer multiples of the elementary charge are screened by vacuum polarization at finite charge densities and their Green function is short ranged. Since only integer charges can be created in the fermionic theory we expect no problems with perturbation expansion at finite density. The second problem, the possibility of dynamical generation of coherent photons, i.e. a background field in the vacuum is more difficult and has to be handled in a self-consistent manner. For this end we introduce an external photon field,

$$\bar{A}^\nu(x^1) = \delta_0^\nu a \cos\left(Qx^1\right), \tag{26}$$

with $a \geq 0$ chosen to be a single plane wave for the sake of simplicity. Since there is only one non-vanishing component of the field strength tensor $F_{\mu\nu} = \partial_\mu A_\nu - \partial_\nu A_\mu$, such a background field represents a generic sinusoidal external field in $1+1$ dimensions. The energy density will be computed in the order $\mathcal{O}(e^4)$ in the vacuum for a given μ and minimized with respect to the external field, the variational parameters a and Q.

The numerical minimization of the vacuum energy density with respect to the background field shows that the system manages to lower the vacuum energy below the 'empty', perturbative value by opening a gap and generating a photon condensate (26) in the vacuum for small densities. For large densities the perturbative treatment of the dependence of the vacuum energy on the field (26) is reliable and yields similar results. Our analysis does not cover the intermediate density regime where the density is large enough to make the numerical minimization of the two-loop energy expression unreliable but small for the application of the perturbation expansion in a.

A. Background field as collective coordinate

The background field is introduced by the collective coordinate method into the generating functional for the Green functions. The vacuum-to-vacuum amplitude of the model is expressed by the path integral

$$Z = \int \mathcal{D}[\bar{\psi}]\mathcal{D}[\psi]\mathcal{D}[A] e^{\mathrm{i}S_{\mathrm{EM}}[A] + \mathrm{i}S_{\mathrm{D}}[A,\bar{\psi},\psi]}, \tag{27}$$

where the action for the photon field A^μ in Feynman gauge,

$$S_{\mathrm{EM}}[A] = -\frac{1}{4}\int_x F^{\mu\nu}F_{\mu\nu} - \frac{1}{2}\int_x (\partial^\mu A_\mu)^2 = \frac{1}{2} A \cdot D^{-1} \cdot A, \tag{28}$$

is expressed in terms of the inverse of the free photon propagator

$$(D^{-1})^{\mu\nu}_{xy} = g^{\mu\nu}\Box_x\delta_{x,y}, \tag{29}$$

and the Dirac action,

$$S_{\rm D}[A,\psi,\bar\psi] = \bar\psi\cdot G^{-1}(A)\cdot\psi, \tag{30}$$

is given by means of the inverse fermion propagator

$$G^{-1}(A) = i\gamma^\mu(\partial_\mu - {\rm i}eA_\mu) - m = \gamma^0 i\partial_0 - H_D(A) \tag{31}$$

with the Dirac Hamiltonian

$$H_D(A) = \gamma^0(-i\gamma^1\partial_1 + m - e\gamma^\mu A_{x\mu}). \tag{32}$$

We use the notation $\int_x = \int_0^T dx^0\int_0^L dx^1$, $f\cdot g = \int_x f_x g_x$ and shall consider the limit $LT\to\infty$ below.

The vacuum of the model will be constructed by means of a variational method. We introduce an external background field $\bar A^\nu_x$ and separate the quantum fluctuations α^ν_x, $A^\nu_x = \bar A^\nu_x + \alpha^\nu_x$. The dependence on the external field is retained by the method of collective coordinates which implies the insertion of the identity

$$1 = \int d\sigma\delta(C[\bar A,\alpha]+\sigma) \tag{33}$$

into the path integral,

$$Z = \int d\sigma Z_\sigma, \qquad Z_\sigma = \int \mathcal{D}[\bar\psi]\mathcal{D}[\psi]\mathcal{D}[\alpha]\delta(C[\bar A,\alpha]+\sigma)e^{{\rm i}S_{\rm EM}[\bar A+\alpha]+{\rm i}S_{\rm D}[\bar A+\alpha,\bar\psi,\psi]} \tag{34}$$

with

$$C[\bar A,\alpha] = \frac14(F-\bar F)\cdot\bar F = \frac12\alpha\cdot D^{-1}\cdot\bar A. \tag{35}$$

The fluctuations of the collective coordinate σ are suppressed in the thermodynamic limit because the background field is extended and the σ-integration can be performed by expanding $\ln Z_\sigma$ around its maximum. The contribution of the collective coordinate to the vacuum energy density will be negligible in the thermodynamic limit and the collective coordinate can be frozen at the maximum as far as the energy density in the vacuum is concerned.

One usually employs the effective action formalism in similar problems. There the external source, coupled linearly to the fluctuating field is supposed to stabilize the vacuum with the desired condensate. The minimization of the effective action guarantees that the external source plays no role in the true vacuum. The complication which renders this method rather involved beyond the leading order of the loop expansion is the Legendre transformation. The procedure outlined above leads to simpler expressions in the two-loop order. Both methods are useful in the case of stable ground state only. Large amplitude fluctuations appear in the mixed phase which make the computation of the convex effective action and the taking into account the fluctuations of the collective coordinate difficult.

It will be useful to introduce the generating functional

$$\begin{aligned} Z[j,\bar\zeta,\zeta] &= \int d\sigma Z_\sigma[j,\bar\zeta,\zeta],\\ Z_\sigma[j,\bar\zeta,\zeta] &= \int d\lambda\int\mathcal{D}[\bar\psi]\mathcal{D}[\psi]\mathcal{D}[\alpha]e^{{\rm i}S_{\rm EM}[\bar A+\alpha]+{\rm i}S_{\rm D}[\bar A+\alpha,\bar\psi,\psi]+{\rm i}\lambda(C[\bar A,\alpha]+\sigma)+{\rm i}j\cdot\alpha+{\rm i}\bar\zeta\cdot\psi+i\bar\psi\cdot\zeta}, \end{aligned} \tag{36}$$

where the constraint is represented as a Fourier integral over λ. The generating functional can be written in the perturbation expansion as

$$Z_\sigma[j,\zeta,\bar\zeta] = \sum_{n=-\infty}^{\infty}\frac{1}{n!}\left({\rm i}e\int_x\frac{\delta}{\delta\zeta^x_\alpha}\gamma^\mu_{\alpha\beta}\frac{\delta}{\delta j^x_\mu}\frac{\delta}{\delta\bar\zeta^x_\beta}\right)^n Z_{0\ \sigma}[j,\zeta,\bar\zeta], \tag{37}$$

where

$$\begin{aligned} Z_{0\ \sigma}[j,\zeta,\bar\zeta] = \exp\Bigg[&{\rm Tr}\ln G^{-1}(\bar A) - {\rm i}\bar\zeta\cdot G(\bar A)\cdot\zeta - \frac{4{\rm i}}{a^2Q^2LT}\sigma^2 - \left(2{\rm i}+4{\rm i}\frac{\bar A\cdot j}{a^2Q^2LT}\right)\sigma\\ &-\frac12{\rm Tr}\ln D^{-1} - \frac12\ln\left(-\frac{Q^2}{4}\bar A\bar A\right) + \frac{\rm i}{2}Q^2\bar A\cdot\bar A - \frac{\rm i}{2}j\cdot D'\cdot j\Bigg] \end{aligned} \tag{38}$$

with

$$D'^{\mu\nu}_{xy} = D^{\mu\nu}_{xy} - \frac{\bar{A}^{\mu}_{y}\bar{A}^{\nu}_{x}}{Q^2\bar{A}\cdot\bar{A}}. \tag{39}$$

The photon propagator (39) tends to the free photon propagator in the thermodynamic limit when the fluctuations parallel to the background field vanish and we continue using the original photon propagator D. Finally, the expectation value of an operator $\hat{\mathcal{O}}[\bar{A}]$ is determined as

$$\mathcal{O}[\bar{A}] = \frac{1}{Z_\sigma[j,\zeta,\bar{\zeta}]}\int d\lambda \int \mathcal{D}[\bar{\psi}]\mathcal{D}[\psi]\mathcal{D}[\alpha]\hat{\mathcal{O}}[\bar{A}]e^{\mathrm{i}S_{\mathrm{EM}}[\bar{A}+\alpha]+\mathrm{i}S_{\mathrm{D}}[\bar{A}+\alpha,\bar{\psi},\psi]+\mathrm{i}\lambda(C[\bar{A},\alpha]+\sigma)+\mathrm{i}j\alpha+\mathrm{i}\bar{\zeta}\psi+\mathrm{i}\bar{\psi}\zeta}\Big|_{j=\zeta=\bar{\zeta}=\sigma=0}, \tag{40}$$

where the field variables in the operator $\hat{\mathcal{O}}[\bar{A}]$ are replaced by functional derivatives with respect to the corresponding external sources.

B. Energy and charge of the vacuum

It may happen that the system prefers energetically a periodic ground state rather than the normal, homogeneous one. Then it should adjust itself by building up a static, periodic electric field and the corresponding band structure with the Fermi-level placed in a forbidden band. In order to decide whether such a readjustment of the vacuum takes place one has to compare the energy densities of the homogeneous and modulated vacua. The fermion spectrum is needed for the determination of the energy and charge densities. It has been calculated along with the corresponding eigenspinors by solving the Dirac equation numerically (see App. A and also App. B for a detailed discussion of the fermion spectrum). The fermion Green functions were constructed according to their Lehmann expansion. The poles on the complex energy plane were shifted according to the rules established in [30] to take into account the chemical potential μ. The energy density $\mathcal{E}[\bar{A}]$ of the system is given by the expectation value of the 00th component of the energy-momentum tensor. At the two-loop order this expectation value can be represented diagrammatically as

$\mathcal{E}[\bar{A}] = \frac{1}{4}a^2Q^2 +$  $-\,\mathrm{i}$ 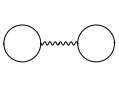 $+\,\mathrm{i}$  $+$ 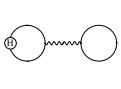 $-$  , (41)

the details of the calculation are given in App. C 1. There is no need of mass and charge renormalizations in QED_{1+1}, but UV and IR divergences appear in the diagrams, which should be properly handled, see App. C 2. We introduce the Casimir energy which is usually the energy difference of the states with and without a classical object and was investigated thoroughly [31] by the collective coordinate method. In our case it is the background field which plays the role of the classical object and the Casimir energy is

$$\mathcal{E}_{\mathrm{C}}(a,Q,\mu) = \mathcal{E}_{\mathrm{per}}(a,Q,\mu) - \mathcal{E}_{\mathrm{n}}(0,0,\mu). \tag{42}$$

In order to understand the structure of the vacuum, we need another important observable, the average charge density ρ. Its two-loop order expectation value is

$\rho[\bar{A}] =$  $+$ 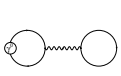 $-$  , (43)

for more details see App. C 3. Charge neutrality for $\mu = 0$ implies the renormalization condition $\rho_{\mathrm{ren}}[\bar{A}\equiv 0] = 0$ which can be satisfied by the subtraction

$$\rho_{\mathrm{ren}}[\bar{A}] = \rho[\bar{A}] - \rho[0]. \tag{44}$$

C. Numerical results

The energy densities given by Eqs. (41) and (42) have been calculated numerically for both the periodic and the homogeneous phases using the explicit formulae of App. C 4 in units of $e = 1$ and the details of the numerical

procedure are discussed in App. C 5. The negative value of the Casimir energy, found numerically, indicates that the periodic state is energetically favoured. The one- and two-loop contributions to the energy are shown in Fig. 6. The one-loop contribution, i.e. that of the first diagram on the r.h.s. of Eq. (41) is more important than the two-loop terms in the parameter range studied. The two-loop correction which is dominated by the exchange diagrams, the third and the fifth ones on the r.h.s of Eq. (41), tends to destabilize the periodic state for $e\mu < m$ and to stabilize it for $e\mu > m$. The periodic phase is stable mainly due to the gain arising from the sinking of upper bands to negative energies and this gain is taken into account completely in our computation since the one-particle energy levels have been calculated non-perturbatively. The photon exchange appearing at the two-loop order becomes important in the region $e\mu \approx m$. The numerical results for $e\mu/m \gtrsim 1.12$ agree for the periodic and the homogeneous ground states within the numerical accuracy.

The computation of the charge density yields the equation of state, the relation between the energy and the charge density. For each μ and m we looked for the values of $a(\mu)$ and $Q(\mu)$ at which the Casimir-energy density assumes its minimum. In this way we obtained $\mathcal{E}_{\rm C}(a(\mu), Q(\mu), \mu) = \mathcal{E}_{\rm C}(\mu)$, and $\rho_{\rm ren}(\mu)$ for each fixed value of m. The equation of state then can be constructed by tracing $\mathcal{E}_{\rm per}(\mu)$ and $\mathcal{E}_{\rm n}(\mu)$ as the function of $\rho_{\rm ren}(\mu)$ for the modulated and the homogeneous phases, respectively. A typical ρ-dependence is shown in Fig. 7 for $m = 2$, similar curves are found for the other values m.

The two-loop results shown in Fig. 7a indicate in a reliable manner that the energy minimum for the periodic ground state, $\mathcal{E}_{\rm per}$, is smaller than that for the homogeneous ground state, $\mathcal{E}_{\rm n}$ for $\rho \in [0, 0.33]$. The amplitude of the periodic background field tends to zero with increasing ρ as one can see in Fig. 7b. Our numerical results for $\rho \lesssim 0.33$ show rapid oscillations in Figs. 7b and c reflecting a numerical problem which arises due to the almost degeneracy found for the periodic states with $Q = k_F$ and $2k_F$. It was found that the wavenumber Q of the periodic phase is directly related to the Fermi momentum k_F via the relation $fQ = 2k_F$, with the filling factor f, defined as the number of the entirely filled positive-energy bands plus the fraction of the partially filled band, see Fig. 8. The ratio Q/k_F displays a discrete behaviour, $Q/k_F \approx 2$ for $e\mu < m$ and $Q/k_F \approx 1$ for $e\mu > m$. The discrete nature of Q/k_F reveals that the vacuum always readjusts itself until a forbidden zone is opened at the Fermi-level and the filling factor becomes integer. This observation is in agreement with the nesting relation $fQ = 2k_F$. The product fQ shown in Fig. 7c increases in the average with increasing charge density, implying the same behaviour of the wavelength as was found in the bosonized theory, c.f. Fig. 5.

For densities larger than the 'critical density' $\rho > 0.33$ we found no energy difference between the periodic and the normal ground state within our numerical accuracy. The reliable numerical determination of the parameters a and Q became impossible, so that those are not shown in Figs. 7b, c for large densities. The result obtained in the framework of the bosonized model, namely the small but non-vanishing amplitude of the modulation of the vacuum for large densities as shown in Fig. 4 makes one cautious that above the 'critical density' the numerical minimization fails to find the proper minimum. But fortunately the smallness of the amplitude of the induced field at large densities enables one to treat the periodic potential as a perturbation. The external potential (26) should open a gap around the Fermi level at $k_F = Q/2$ according to the leading order of the degenerate perturbation expansion [32] and one finds the energy spectrum

$$\epsilon_k^{\pm} = \frac{1}{2}\left[\epsilon_k^{(0)} + \epsilon_{k-Q}^{(0)} \pm \sqrt{(\epsilon_k^{(0)} - \epsilon_{k-Q}^{(0)})^2 + 4e^2a^2}\right], \tag{45}$$

close to the quasi-momentum $k \approx k_F$, where $\epsilon_k^{(0)}$ refers to the unperturbed spectrum and the signs + and − stand for $|k| > \frac{1}{2}Q$ and $|k| < \frac{1}{2}Q$, respectively. Due to the first order perturbation treatment we can now ignore the two-loop order diagrams in Eq. (41). By means of the energy eigenvalues in Eq. (45) one finds

$$\mathcal{E}_{\rm C}(a, Q, \mu) = \frac{1}{4}a^2Q^2 + \underset{\rm per}{\left(\text{H}\right)} - \underset{\rm n}{\left(\text{H}\right)} = \frac{1}{4}a^2Q^2 + \int_{-Q/2}^{Q/2}\frac{{\rm d}k'}{2\pi}\epsilon^-_{\frac{1}{2}Q-k'} - \int_{-Q/2}^{Q/2}\frac{{\rm d}k'}{2\pi}\epsilon^{(0)}_{\frac{1}{2}Q-k'}, \tag{46}$$

for the Casimir-energy density in the leading order. Since $\rho = \int_{-k_F}^{k_F} dk/2\pi = k_F/\pi$ and $Q/2 = k_F = \pi\rho$ we have $\rho = Q/2\pi$. For large values of the chemical potential μ we expect large values of $k_F = Q/2 \gg m$ therefore we can set $m = 0$, i.e. $\epsilon^{(0)}(k) = |k|$, $\mu = k_F = Q/2$ and one can perform the integral in Eq. (46) explicitly,

$$\mathcal{E}_{\rm C}(a, Q, Q/2) = \frac{Q^2}{8\pi} + \frac{1}{4}a^2Q^2 - \frac{Q\sqrt{Q^2 + 4e^2a^2}}{8\pi} - \frac{e^2a^2}{2\pi}{\rm arsinh}\frac{Q}{2ea}. \tag{47}$$

For a given Q, i.e. ρ the Casimir-energy density has two extrema: a maximum at $a = 0$ ($\partial_a^2\mathcal{E}_{\rm C}(0, Q, Q/2) \to -\infty$) and a minimum at

$$a_{\min} = \frac{Q}{2e\sinh(\frac{\pi Q^2}{2e^2})} = \frac{\pi\rho}{e\sinh(\frac{2\pi^3\rho^2}{e^2})} > 0 \tag{48}$$

($\partial_a^2 \mathcal{E}_{\rm C}(a_{\min}, Q, Q/2) > 0$). The latter provides the Casimir-energy density of the ground state,

$$\mathcal{E}_{\rm C}(a_{\min}, Q, Q/2) = \frac{Q^2}{8\pi}\left[1 - \sqrt{1 + \frac{4e^2 a_{\min}^2}{Q^2}}\right] = \frac{\pi\rho^2}{2}\left[1 - \coth\frac{2\pi^3\rho^2}{e^2}\right] < 0. \tag{49}$$

One finds $a_{\min} \approx 0.004$ and $\mathcal{E}_{\rm C}(a_{\min}, 2\pi\rho, \pi\rho) \approx -10^{-5}$ at the 'critical density' $\rho = 0.33$ therefore it is not possible to confirm the periodicity of the ground state within our numerical accuracy. Furthermore we have seen for lower densities that the jump from one band to two bands in the Dirac sea is a two-loop effect caused by photon exchange. In general, one needs higher-loop corrections in order to let more than two bands sinking into the Dirac sea. This is due to the observation that the N-th order perturbation expansion in the monochromatic external field predicts the opening of N gaps in the fermion spectrum. Nevertheless this simple computation indicates that the vacuum of the massive Schwinger model keeps its periodicity, although with decreasing amplitude $a \sim \rho e^{-2\pi^3\rho^2/e^2}$ and wavelength $2\pi/Q = 1/\rho$ for increasing charge density ρ, in a manner similar to the bosonized model (see Fig. 5). The one-loop level vacuum for the assumed simple sinusoidal background potential involves a single band sunk into the Dirac sea.

For the low-density periodic phase $e\mu \approx m$ where the amplitude a is non-perturbative the photon exchange is significant. As ρ increases the perturbative region of a is reached, although we could not decide, whether the numerically found 'critical density' does fall into the perturbative region. Our one-loop perturbative result cannot clarify whether higher-order loop corrections can lead to sinking more and more bands into the Dirac sea as the density ρ increases.

IV. SUMMARY

The ground state for the massive Schwinger model has been investigated in the presence of homogeneous external charge density. The energy density of the ground state has been determined numerically in the bosonized version of the model as well as in terms of the original degrees of freedom of QED by variational methods. The scalar field configuration and the charge density of the ground state for the bosonized model have been obtained by minimizing the tree-level energy in the presence of static, homogeneous external charge density. In the fermionic theory a variational method has been constructed by minimizing for the amplitude and the wavelength of a sinusoidal photon condensate in the vacuum. The finite charge density was realized by the introduction of the chemical potential. The applicability of the loop-expansion for the computation of the vacuum energy at finite density is justified by the bosonized theory which indicates that the confining Coulomb-force among integer charges is vanishing.

The computation in the bosonized theory shows that the system exhibits a periodic ground state for arbitrary charge density. The fermionic computation gives the same result. Numerical computations reliable up to a certain charge density as well as simple analytic calculations valid for asymptotically large charge densities support the periodicity of the ground state. The general trends in the charge-density dependence of the amplitude and that of the wavelength of the periodic structure are in agreement for both versions of the model.

The investigations in terms of the bosonic and fermionic degrees of freedom complement each other. On the one hand, our results for the bosonized model showed that the background charge density is in average neutralized in the ground state. Furthermore, the charge density wave ground state and the complete screening of the integer charges appear due to the interplay of the kinetic energy, the periodic potential energy and that of the boundary condition for the boson field. The fermionic description, on the other hand, gives more insight into the structure of the vacuum, namely that the modulation of the charge density arises as the result of the opening of a gap in the fermion spectrum. The conclusion of the straightforward perturbation expansion for large charge densities is that the periodic ground state is always favoured by the system energetically as compared to the homogeneous one, even if only a single band sinks into the Dirac sea. In the case of a single mode periodic potential N bands sink below the Fermi-level in the N-th order of the perturbation expansion. In particular, in our numerical computation where a single mode was allowed for the induced photon field in the vacuum and first (second) order perturbation expression for the vacuum energy was minimized one (two) bands are found below the Fermi-level for large densities. The Peierls mechanism is present in the relativistic vacuum for $N \geq 2$. It is however not clear how to identify this mechanism in terms of the bosonic excitations.

Our analytic considerations showing the existence of the periodic ground state for arbitrarily large charge densities do not include the corresponding higher-order loop corrections neither for the bosonized model, nor for the fermionic one. It still remains an open question whether a complete resummation of these higher-order corrections would alter the qualitative result obtained here, namely that the massive Schwinger model has only a single phase, the periodic one for any values of the average charge density.

ACKNOWLEDGEMENTS

This work has been supported by the grants OTKA T032501/00, NATO SA(PST.CLG 975722)5066, and also partially by the grant OTKA M041537 and the Supercomputing Laboratory of the Faculty of Natural Sciences, University of Debrecen. One of us (K.S.) has been supported by the Alexander von Humboldt-Foundation and he thanks W. Greiner for the kind hospitality and the impetus given by him to study strongly interacting vacua and also thanks J. Csikai making him aware of Ref. [33] in the general physics lectures nearly three decades ago.

---

[1] C. G. Callen, R. F. Dashen, D. J. Gross, Phys. Lett. **63B** (1976) 334; R. Jackiw, C. Rebbi, Phys. Rev. Lett. **37** (1976) 172.
[2] I. A. Batalin, S. G. Matinyan, G. K. Savvidy, Sov. J. Nucl. Phys. **26** (1977) 214; G. K. Savvidy, Phys. Lett. **71B** (1977) 133.
[3] J. Alexandre, V. Branchina, J. Polonyi, Phys. Lett. **B445** (1999) 351.
[4] E. P. Wigner, Phys. Rev. **46** (1934) 1002
[5] G. Grüner, *Density Waves in Solids* (Addison Wesley, New York, 1994); G. Grüner and A. Zettl, Phys. Rep. **119** (1985) 117
[6] J. Schwinger, Phys.Rev. **82** (1951) 664
[7] G. Kohring, R. E. Shrock, Nucl. Phys. **B295** (1988) 36; S. Caracciolo, R. G. Edwards, A. Pelisetto, A. D. Sokal, Nucl. Phys. B Proc. Suppl. **30** (1933) 815; J. L. Alonso, A. Tarancon, H. G. Ballesteros, L. A. Fernandez, V. Martin-Mayor, A. Munoz Sudupe, Phys. Rev. **B53** (1966) 2537; M. L. Plummer, A. Caille, J. of Appl. Phys. **70** (1991) 5961; H. Kawamura, J. Phys. Soc. Jpn. **61** (1992) 1299; H. G. Ballesteros, L. A. Fernandez, V. Martin-Mayor, A. Munoz Sudupe, Phys. Lett. **B378** (1966) 207; Nuc. Phys. **B483** (1977) 707; P. Azaira, B. Delamotte, F. Delduc, T. Jolicoeur, Nucl. Phys. **B408** (1993) 485; J. L. Alonso, J. M. Carmona, J. Clemente Gallardo, L. A. Fernandez, D. Iniguez, A. Tarancon, C. L. Ullod, Phys. Lett. **B376** (1996) 148; I. Campos, L. A. Fernandez, A. Tarancon, Phys. Rev. **D55** (1977) 2965; H. G. Ballesteros, J. M. Carmona, L. A. Fernandez, V. Martin-Mayor, A. Munoz Sudupe, A. Tarancon, Phys. Rev. **D55** (1977) 5067; Y. Shamir, hep-lat/9512019; J. Fingberg, J. Polonyi, Nucl. Phys. **B486** (1997) 315; V. Branchina, H. Mohrbach, J. Polonyi, Phys. Rev. **D60** (1999) 45006; Phys. Rev. **D60** (1999) 45007; M. Dufour Fournier, J. Polonyi, Phys. Rev. **D61** (2000) 065008.
[8] J. Schwinger, Phys.Rev. **125** (1962) 397, ibid. Phys. Rev. **128** (1962) 2425
[9] S. Coleman, R. Jackiw, L. Susskind, Annals of Physics **93** (1975) 267
[10] H. J. Rothe, K. D. Rothe, J. A. Swieca, Phys. Rev. D**19** (1979) 3020
[11] W. Fischler, J. Kogut, L. Susskind Phys. Rev. **D19** (1979) 1188
[12] D. V. Deriagin, D. Yu. Grigoriev, V. A. Rubakov, Int. J. Mod. Phys. A**47** (1992) 659
[13] V. Schön, M. Thies, Phys.Rev. D**62** (2000) 096002 M. Thies, Phys.Rev. D**69** (2004) 067703, O. Schnetz, M. Thies, K. Urlichs, hep-th/0402014
[14] H. R. Christiansen, F. A. Schaposnik, Phys. Rev. D**55** (1997) 4920
[15] R. Comès, M. Lambert, H. Launois, H. R. Zeller, Phys. Rev. **B8** (1973) 571
[16] J. Hubbard, Phys. Rev. B**17** (1978) 494
[17] H. J. Schulz, Phys. Rev. Lett. **71** (1993) 1864
[18] R. E. Peierls, *Quantum Theory of Solids* (Clarendon Press, Oxford, 1955)
[19] B. E. Baaquie, J. Phys G: Nucl. Phys. **8** (1982) 1621
[20] S. Coleman Phys.Rev. **D11** (1975) 2088
[21] J. H. Lowenstein, J. A. Swieca, Annals of Physics **68** (1971) 172
[22] S. Coleman, Annals of Physics **101** (1976) 239
[23] A. Casher, J. Kogut, L. Susskind, Phys. Rev. **D10** (1976) 732
[24] J. Kijowski, [arXiv:]hep-th/9710003
[25] Y.-C. Kao, Y.-W. Lee, Phys. Rev. **D50** (1994) 1165
[26] H. R. Christiansen, F. A. Schaposnik, Phys. Rev D**53** (1996) 3260
[27] Y. I. Frenkel, T. Kontorowa, Zh. Eksp. Teor. Fiz. **8** (1938) 1340; F. C. Frank, J. H. van der Merwe, Proc. Roy. Soc. London **198** (1949) 205.
[28] S. Aubry, in *Solitons in Condensed Matter Physics*, eds. A. R. Bishop, T. Schneider (Springer, New-York, 1978).
[29] S. Nagy, J. Polonyi, K. Sailer Heavy Ion Phys., Proc. Non-Euclidean Geometry in Modern Physics (2002) 73
[30] R. Anishetty, J. Phys. **G 10** (1984) 423
[31] M. Bordag, D. Robaschik, E. Wieczorek, Ann. Phys. (N.Y.) **165** (1985) 192, D. Robaschik, K. Scharnhorst, E. Wieczorek, Ann. Phys. (N.Y.) **174** (1987) 401

[32] L. Landau, M. Lifshitz, *Course of Theoretical Phys. Vol. 9.* (Pergamon Press, Oxford, 1971)
[33] J. C. Slater, Phys. Rev. **87** (1952) 807
[34] I.S. Gradstein, I.M. Ryzhik, *Table of Integrals, Series and Products* (Academic Press, New York, 1965); William H. Press, Brian P. Flannery, Saul A. Teukolsky, William T. Vetterling *Numerical Recipes in C : The Art of Scientific Computing* (Cambridge Univ. Press. Cambridge, 1992)
[35] Tara Prasad Das, *Relativistic Quantum Mechanics of Electrons* (Harper & Row, Pulishers New York, 1973)
[36] J. I. Kapusta, Nucl. Phys. B**148** (1979) 461
[37] T. Toimela, Int. J. Th. Phys. **24** (1985) 901
[38] B. A. Freedman, L. D. McLerran, Phys. Rev. **D16** (1977) 1130; ibid., Phys. Rev. **D16** (1977) 1147

APPENDIX A: DIRAC EQUATION WITH SINUSOIDAL POTENTIAL

The Lehmann representation of the non-interacting electron propagator requires the knowledge of the eigenfunctions of the Dirac Hamiltonian (32) for the external field (26). We use the real Dirac matrices

$$\gamma^0 = \begin{pmatrix} 1 & 0 \\ 0 & -1 \end{pmatrix}, \qquad \gamma^1 = \begin{pmatrix} 0 & 1 \\ -1 & 0 \end{pmatrix}. \tag{A1}$$

The eigenspinors $f^{ks}(x)$ and $g^{ks}(x)$ of the Dirac Hamiltonian $H_D(\bar{A})$ belonging to the positive and negative energy eigenvalues $\epsilon_{ks}^{(+)}>0$ and $-\epsilon_{ks}^{(-)}<0$, respectively satisfy the equations

$$H_D(\bar{A})\ f^{ks}(x) = \epsilon_{ks}^{(+)}\ f^{ks}(x), \qquad H_D(\bar{A})\ g^{ks}(x) = -\epsilon_{ks}^{(-)}\ g^{ks}(x), \tag{A2}$$

where the quasi-momentum $k \in [-Q/2, Q/2)$ takes values in the first Brillouin-zone. The non-negative integer $s \geq 0$ labels the bands in increasing order in the energy. As in the non-relativistic case, the solutions of Eq. (A2) are Bloch-waves,

$$f^{ks} = \sum_{n=-\infty}^{\infty} u_n^{ks} e^{-\mathrm{i}\left(\epsilon_{ks}^{(+)} x_0 - k_n x_1\right)}, \qquad g^{ks} = \sum_{n=-\infty}^{\infty} v_n^{ks} e^{\mathrm{i}\left(\epsilon_{ks}^{(-)} x_0 - k_n x_1\right)}, \tag{A3}$$

with $k_n{=}k{+}nQ$. In order to find the numerical solution, one rewrites Eqs. (A2) in matrix forms for the components of the Bloch-waves, e.g. the first one of Eqs. (A2) reads as

$$\sum_{n=-\infty}^{\infty} \left[\left(\epsilon_{ks} + e\mu - k_n \gamma^0\gamma^1 - m\gamma^0\right) u_n^{ks} + \frac{ea}{2}\left(u_{n+1}^{ks} + u_{n-1}^{ks}\right) \right] e^{-\mathrm{i}(\epsilon_{ks} x_0 - k_n x_1)} = 0. \tag{A4}$$

The solution is found by making up a matrix from the coefficients appearing next to the Dirac spinors u_n^{ks}. The non-relativistic treatment results in a matrix with tridiagonal structure [33], [34]. The structure of the matrix remains unchanged in the relativistic case except of the replacement of the matrix elements with 2×2 matrices. The problem is then reduced to solve a system of a coupled set of homogeneous linear equations.

APPENDIX B: BAND STRUCTURE

In order to understand the effects of the photon exchanges, the salient features of non-interacting electrons in static periodic background field are briefly summarized in this section. The eigenspinors and the energy eigenvalues of the Dirac Hamiltonian (32) in the static, periodic external field have been determined numerically (App. A). The positive and negative single-particle energies are denoted by $\epsilon_{ks}^{(+)}$ and $-\epsilon_{ks}^{(-)}$, respectively, as the functions of the quasi-momentum k and the band index s. Their dependences on the parameters a, Q are not indicated explicitly. Since the chemical potential μ results in a constant shift of the whole fermion spectrum, it is sufficient to understand the spectrum for $\mu = 0$. Due to the periodic potential, a band structure with alternating allowed and forbidden bands is formed [35]. The typical band structure is plotted in Fig. 9a and 9b as the function of $1/Q$ for undercritical $ea < m$ and overcritical $ea > m$ static periodic external electric fields, respectively. The shaded regions in Figs. 9 correspond to the allowed bands. The non-relativistic analogue of these figures can be found in [33] where the one-dimensional electron system was considered in the presence of the static external electric potential $A_0 = a(1 - \cos Qx)$ (with our notations) that is just the same potential we have but one of its minima is shifted to $x = 0$ and the potential is chosen zero in this minimum. The following qualitative features of the fermion spectrum are wothwhile mentioning.

1. Undercritical vacuum $ea<m$: The mass gap around zero energy separates the infinite towers of bands above and below this gap. The smaller is $1/Q$, the more the allowed bands widen out and start to overlap. This is just the qualitative behaviour obtained in the non-relativistic description [33]. The energies of the states in the upper, $\epsilon > 0$ (lower, $\epsilon < 0$) tower decrease (increase) with increasing $1/Q$.

2. Overcritical vacuum $ea > m$: The qualitative features described above remain the same but the upper and the lower bands overlap for large enough $1/Q$ and upper bands sink into the Dirac sea while lower bands emerge. The band crossing is well understood [29] but this case which involvs the creation of electron-positron pairs turned out to be not relevant for our purpose because the periodic ground state was found undercritical.

The asymptotics of the spectrum for $1/Q \to 0$ and $1/Q \to \infty$ is helpful to understand the $1/Q$-dependence of the band structure.

1. $1/Q \to 0$: The energy levels decouple from the periodic structure of the potential and the free fermion spectrum reappears with the single gap for $-m \leq \epsilon \leq m$. This can easily understood by noticing that the potential term in the Dirac Hamiltonian (32) becomes negligible compared to the kinetic energy for $Q \to \infty$. In fact, the introduction of the rescaled coordinate $\xi_1 = Qx_1$ leaves the only Q-dependence coming from the gradient term of the Hamiltonian. This corresponds to infinitely densely packed atoms in the model of Ref. [33] and to vanishing average electric potential.

2. $1/Q \to \infty$: The extrema of the potential is now well-separated and one expects localized states at the minima (maxima) corresponding to the upper (lower) bands. Furthermore each band should be reduced to a single, highly degenerate energy level which corresponds to the localized states at the various minima (maxima) of the external potential. The semiclassical tunneling probability from a minimum to the neighbouring one is suppressed exponentially with increasing $1/Q$, $w \sim \exp\{-16\sqrt{mea}/Q\}$ and the problem reduces to that of the relativistic harmonic oscillator as far as the lowest (highest) lying states of the upper (lower) band are concerned [29].

The dispersion relations in the allowed bands alternate between convex and concave ones from band to band. If the Fermi-level lies inside of an allowed band, the occupied states build either a Fermi sphere or a Fermi hole in momentum space. For one spatial dimension the Fermi sphere is distorted to a Fermi section $p_1 \in [-k_F, k_F]$, the Fermi hole appears as the unoccupied interval $p_1 \in [-k_F, k_F]$ between the occupied ones, $p_1 \in [-Q/2, -k_F]$ and $p_1 \in [k_F, Q/2]$.

APPENDIX C: NUMERICAL CALCULATION OF THE ENERGY AND CHARGE DENSITY

This appendix contains the details of the calculations of the energy and charge density.

1. Bare expression for the energy density

The effective Lagrangian corresponding to the action (36),

$$\mathcal{L} = -\frac{1}{4}F_{\rho\sigma}F^{\rho\sigma} + \frac{1}{2}\bar{\psi}i\gamma^\rho\partial_\rho\psi - \frac{1}{2}\partial_\rho\bar{\psi}i\gamma^\rho\psi + e\bar{\psi}\gamma^\rho A_\rho\psi - m\bar{\psi}\psi + \lambda\frac{1}{4}(F-\bar{F})_{\rho\sigma}\bar{F}^{\rho\sigma} \tag{C1}$$

yields the energy-momentum tensor,

$$T^{\mu\nu} = \frac{\partial\mathcal{L}}{\partial(\partial_\mu A^\kappa)}\partial^\nu A^\kappa - \frac{\partial\mathcal{L}}{\partial(\partial_\mu\psi)}\partial^\nu\psi + \partial^\mu\bar{\psi}\frac{\partial\mathcal{L}}{\partial(\partial_\nu\bar{\psi})} + \lambda\bar{F}^{\mu\kappa}\partial^\nu A_\kappa - g^{\mu\nu}\mathcal{L}, \tag{C2}$$

which should be symmetrized by adding the divergence $-\partial_\rho f^{\nu\rho\mu}$ of the third rank tensor

$$f^{\nu\mu\rho} = F^{\mu\rho}A^\nu + \frac{\mathrm{i}}{8}\bar{\psi}(\gamma^\mu\gamma^\nu\gamma^\rho - \gamma^\rho\gamma^\nu\gamma^\mu)\psi, \tag{C3}$$

determined by the spin density,

$$T^{\mu\nu}_{\mathrm{sym}} = T^{\mu\nu} - \partial_\rho f^{\nu\rho\mu} = -F^{\mu\rho}F^\nu_\rho + \lambda\bar{F}^{\mu\kappa}\partial^\nu A_\kappa + \frac{\mathrm{i}}{4}(\bar{\psi}\gamma^\mu\partial^\nu\psi + \bar{\psi}\gamma^\nu\partial^\mu\psi) - \frac{\mathrm{i}}{4}(\partial^\nu\bar{\psi}\gamma^\mu\psi + \partial^\mu\bar{\psi}\gamma^\nu\psi) - g^{\mu\nu}\mathcal{L}. \tag{C4}$$

It is easy to see that the symmetrized energy-momentum tensor is gauge invariant. The energy density operator is

$$\hat{\mathcal{E}}[A,\bar{\psi},\psi] = \frac{1}{LT}\int_x T^{00}_{\rm sym} = \frac{1}{LT}\int_x \left[\frac{1}{2}(F^{01}_x)^2 - \bar{\psi}_x H_D(A)\psi_x + \lambda \bar{F}^{0\kappa}\partial^0 A_\kappa - \frac{\lambda}{4}(F-\bar{F})_{\rho\sigma}\bar{F}^{\rho\sigma}\right], \tag{C5}$$

where the first term on the r.h.s. is the energy density of the photons and the second one is the energy density of the Dirac sea minus $e\mu$ multiplied by the fermion density. The last two terms appear due to the exclusion of the fluctuations of the collective mode. One can write $\hat{\mathcal{E}} = \hat{\mathcal{E}}_{(0)} + \hat{\mathcal{E}}_{(1)} + \hat{\mathcal{E}}_{(2)}$ with

$$\begin{aligned}
\hat{\mathcal{E}}_{(0)}[\bar{A},\bar{\psi},\psi,\lambda] &= \frac{1}{LT}\int_x \left[\frac{1}{2}(\bar{F}^{01}_x)^2 + \lambda\bar{F}^{0\kappa}\partial^0\bar{A}_\kappa - \bar{\psi}_x H_D(\bar{A})\psi_x\right],\\
\hat{\mathcal{E}}_{(1)}[\bar{A},\alpha,\bar{\psi},\psi,\lambda] &= \frac{1}{LT}\int_x \alpha_{\mu x}\left(-g^{\mu 1}\partial^0_x\bar{F}^{01}_x + g^{\mu 0}\partial^1_x\bar{F}^{01} + \frac{\lambda}{2}\Box_x\bar{A}^\mu_x - \lambda\partial^0_x\bar{F}^{0\mu}_x - e\bar{\psi}\gamma^\mu\psi\right),\\
\hat{\mathcal{E}}_{(2)}[\alpha] &= \frac{1}{LT}\int_x \frac{1}{2}[(g^{\mu 1}\partial^0 - g^{\mu 0}\partial^1)\alpha_{\mu x}][(g^{\nu 1}\partial^0 - g^{\nu 0}\partial^1)\alpha_{\nu x}],
\end{aligned} \tag{C6}$$

where the lower indices indicate the powers of α. According to Eq. 40, the expectation value of the operator $\hat{\mathcal{E}}$ in the vacuum is given as $\mathcal{E}[\bar{A}] = \sum_{i=0}^2 \mathcal{E}_{(i)}[\bar{A}]$. We find

$$\begin{aligned}
\mathcal{E}_{(0)}[\bar{A}] = &\frac{1}{4}Q^2a^2 + \frac{1}{Z}\int_x \frac{\delta}{\mathrm{i}\delta\zeta^x_\alpha}\hat{H}_D(\bar{A})_{\alpha\beta}\frac{\delta}{\mathrm{i}\delta\bar{\zeta}^x_\beta}Z_0|_{j=\zeta=\bar{\zeta}=0}\\
&-\frac{e^2}{2Z}\int_x \frac{\delta}{\mathrm{i}\delta\zeta^x_\alpha}\hat{H}_D(\bar{A})_{\alpha\beta}\frac{\delta}{\mathrm{i}\delta\bar{\zeta}^x_\beta}\int_{y,z}\frac{\delta}{\delta\zeta^y_\kappa}\gamma^\mu_{\kappa\lambda}\frac{\delta}{\delta j^y_\mu}\frac{\delta}{\delta\bar{\zeta}^y_\lambda}\frac{\delta}{\delta\zeta^z_\epsilon}\gamma^\nu_{\epsilon\delta}\frac{\delta}{\delta j^z_\nu}\frac{\delta}{\delta\bar{\zeta}^z_\delta}Z_0|_{j=\zeta=\bar{\zeta}=0}\\
= &\frac{1}{4}Q^2a^2 + \frac{1}{Z}\Bigg[
\end{aligned}$$

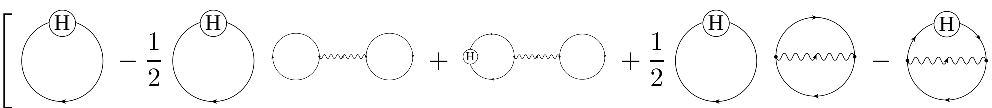

$$\Bigg] \tag{C7}$$

with

$$Z_0 = \exp\left\{-\frac{\mathrm{i}}{2}j\cdot D\cdot j - \mathrm{i}\bar{\zeta}\cdot G(\bar{A})\cdot\zeta\right\}, \tag{C8}$$

and $\hat{H}_D(\bar{A})$ denoting the Dirac Hamiltonian (32) with the field variables replaced by functional derivatives with respect to the corresponding external sources, and the vacuum-to-vacuum amplitude up to the order $\mathcal{O}(e^2)$ is

$$\begin{aligned}
Z &= 1 - \frac{e^2}{2}\int_{x,y}\frac{\delta}{\delta\zeta^x_\alpha}\gamma^\mu_{\alpha\beta}\frac{\delta}{\delta j^x_\mu}\frac{\delta}{\delta\bar{\zeta}^x_\beta}\frac{\delta}{\delta\zeta^y_\epsilon}\gamma^\nu_{\epsilon\delta}\frac{\delta}{\delta j^y_\nu}\frac{\delta}{\delta\bar{\zeta}^y_\delta}Z_0|_{j,\zeta,\bar{\zeta}=0}\\
&= 1 - \frac{1}{2}\Bigg[
\end{aligned}$$

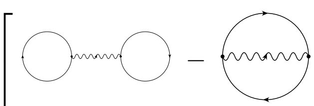

$$\Bigg]. \tag{C9}$$

The $\mathcal{O}(\alpha^0)$ energy, Eq. (C7), includes the energy density of the background and those of the modulated, interacting Dirac-sea. The $\mathcal{O}(\alpha)$ energy term is the interaction energy of the current with the fluctuations of the photon field,

$$\begin{aligned}
\mathcal{E}_{(1)}[\bar{A}] &= -\frac{\mathrm{i}e^2}{Z}\int_{x,y}\frac{\delta}{\mathrm{i}\delta\eta^x_\alpha}\gamma^\mu_{\alpha\beta}\frac{\delta}{\mathrm{i}\delta j^x_\mu}\frac{\delta}{\mathrm{i}\delta\bar{\eta}^x_\beta}\frac{\delta}{\mathrm{i}\delta\eta^y_\alpha}\gamma^\nu_{\alpha\beta}\frac{\delta}{\mathrm{i}\delta j^y_\nu}\frac{\delta}{\mathrm{i}\delta\bar{\eta}^y_\beta}Z_0|_{j=\eta=\bar{\eta}=0}\\
&= -\frac{\mathrm{i}}{Z}\Bigg[
\end{aligned}$$

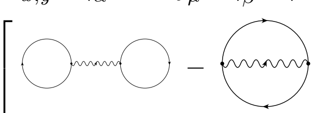

$$\Bigg]. \tag{C10}$$

The $\mathcal{O}(\alpha^2)$ energy expression depends on the fluctuating field α only. Since the photon propagator in the presence of the background field approaches the free propagator as $L\to\infty$ the contribution $\mathcal{E}_{(2)}$ cancels when the difference of the energy densities with and without the background field is considered. The vacuum to vacuum amplitude removes the disconnected components as expected and one finds

$$\mathcal{E}[\bar{A}] = \frac{1}{4}a^2Q^2 + \quad - \mathrm{i} \quad + \mathrm{i} \quad + \quad - \quad . \tag{C11}$$

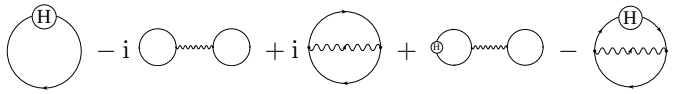

The propagators are calculated by means of the Lehmann representation

$$G^{\alpha\beta}_{xy} = \sum_{k_1 s_1} \int \frac{dk_0}{2\pi} e^{-\mathrm{i}k_0(x_0-y_0)} \Big[\frac{f^{k_1 s_1}_\alpha(x)\bar{f}^{k_1 s_1}_\beta(y)}{k_0 + i\varepsilon} + \frac{g^{k_1 s_1}_\alpha(x)\bar{g}^{k_1 s_1}_\beta(y)}{k_0 - i\varepsilon} \Big], \qquad D^{\mu\nu}_{xy} = -g_{\mu\nu} \sum_{k_1} \int \frac{dk_0}{2\pi} \frac{1}{k^2 + i\varepsilon} e^{\mathrm{i}k(x-y)}, \tag{C12}$$

where $f^{k_1 s_1}(x)$ and $g^{k_1 s_1}(x)$ denote the positive and negative energy eigensolutions of the Dirac-equation (see App. A). The periodic background potential breaks the translational symmetry which manifests itself in changing momentum conservation to quasi-momentum conservation in each vertex.

2. UV and IR divergences

The first diagram on the r.h.s. of Eq. (C11) represents the energy of the Dirac-sea in the presence of the background field,

$$\mathcal{E}_{\mathrm{sea}}(a,Q,\mu) = \quad = \frac{1}{LT} \int dx \gamma^0_{\alpha\beta} \hat{H}^{x(\beta)}_D(\bar{A}) \mathrm{i} G^{\beta\alpha}_{xx} = -\frac{1}{LT} \sum_{k_1 s_1} \epsilon^{(-)}_{k_1 s_1}, \tag{C13}$$

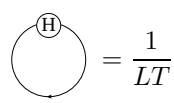

and is quadratically divergent in the absence of the background field,

$$\mathcal{E}_{\mathrm{sea}}(0,0,0) = -\int_{-\Lambda}^{\Lambda} \frac{\mathrm{d}p}{2\pi} \left[p^2 + m^2\right]^{1/2}. \tag{C14}$$

The finite, physical part of $\mathcal{E}_{\mathrm{sea}}$ will be defined by

$$\mathcal{E}^{(1-l)}_{\mathrm{per}}(a,Q,\mu) = \mathcal{E}_{\mathrm{sea}}(a,Q,\mu) - \mathcal{E}_{\mathrm{sea}}(0,0,0), \qquad \mathcal{E}^{(1-l)}_{\mathrm{n}}(\mu) = \mathcal{E}_{\mathrm{sea}}(0,0,\mu) - \mathcal{E}_{\mathrm{sea}}(0,0,0) \tag{C15}$$

for the periodic and the homogeneous, normal phases, respectively.

The convergence of $\mathcal{E}_{\mathrm{per}}$ was checked numerically in the following manner. The one-loop contributions are obtained by taking $\mathcal{E}$ of Eq. (C13) for the background field and subtracting from it the same diagram without background field. Let us consider first this difference for vanishing chemical potential $\mu = 0$,

$$\mathcal{E}^{(1-l)}_{\mathrm{per}}(a,Q,0) = -\frac{1}{LT} \sum_{k_1\ s_1} [\epsilon^{(-)}_{k_1\ s_1}(a,Q,0) - \epsilon^{(-)}_{k_1\ s_1}(0,0,0)]. \tag{C16}$$

By the one-by-one identification of the corresponding levels we found numerically that the magnitude $|\epsilon_{k_1\ s_1}(a,Q,0) - \epsilon_{k_1\ s_1}(0,0,0)|$ is suppressed for increasing k_1 according to the power law

$$|\epsilon^{(-)}_{k_1\ s_1}(a,Q,0) - \epsilon^{(-)}_{k_1\ s_1}(0,0,0)| \approx k_1^{-(1+\delta)} \tag{C17}$$

with $\delta \approx 2 > 0$, cf. Fig. 10. This renders the sum absolutely convergent. The shift in the spectrum caused by the non-vanishing chemical potential does not alter the UV behaviour of the sum even in the thermodynamic limit. The convergence of $\mathcal{E}_{\mathrm{n}}(\mu) = \mathcal{E}(0,0,\mu) - \mathcal{E}(0,0,0)$ has been checked similarly.

IR divergences can also appear at the tadpoles where the photon line carries vanishing momentum $q^\mu = 0$. Since there is actually no dynamical photon-field variable with vanishing energy and momenta, such tadpoles pose no problem in the homogeneous, normal vacuum [36–38]. In the periodic vacuum the photon can borrow the momentum nQ from the vacuum by the summation for $n \neq 0$ and the tadpoles are finite.

3. Charge density

In order to understand the structure of the vacuum, we need another important observable, the average charge density ρ given as the two-loop order expectation value of the operator

$$\hat{\rho} = \frac{1}{LT}\int_x \bar{\psi}\gamma^0\psi. \tag{C18}$$

The expectation value of $\rho[\bar{A}]$ is taken by Eq. (40), and truncated at the two-loop order is given as

$\rho[\bar{A}] =$ 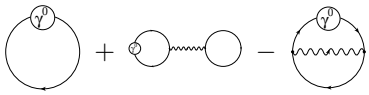 . (C19)

These diagrams are similar to the first, fourth and fifth ones of Eq. (C11) except that the Hamiltonian-insertion is replaced by a γ^0-insertion. The renormalization prescription (44) removes the UV divergence of the first diagram in Eq. (C19), too. The second diagram gives vanishing contribution for vanishing periodic background electric field due to Furry's theorem. The calculation of these diagrams proceeds like those for the Casimir-energy density.

4. Two-loop diagrams

We present now the explicit expressions for the two-loop diagrams on the r.h.s. of Eq. (41). The eigenspinors u and v are defined in Eq. (A3) and the diagrams containing tadpoles are

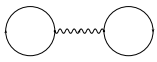
$$\begin{aligned}
&= -\frac{\mathrm{i}e^2}{LT}\int_{x,y} \mathrm{i}D^{yx}_{\nu\mu}\gamma^\nu_{\alpha\beta}\mathrm{i}G^{xx}_{\beta\alpha}\gamma^\mu_{\epsilon\delta}\mathrm{i}G^{yy}_{\delta\epsilon} \\
&= \frac{e^2}{LT}\sum_{q_1}\frac{1}{|q_1|^2}\sum_{\substack{k_1,s_1\\ n_1,n_2}} \bar{v}^{k_1s_1}_{\alpha n_1}\gamma^\mu_{\alpha\beta}v^{k_1s_1}_{\beta n_2}\delta(q_1+(n_1-n_2)Q)\sum_{\substack{k_1,s_1\\ n_1,n_2}} \bar{v}^{k_1s_1}_{\epsilon n_1}\gamma^\mu_{\epsilon\delta}v^{k_1s_1}_{\delta n_2}\delta(-q_1+(n_1-n_2)Q),
\end{aligned} \tag{C20}$$

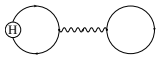
$$\begin{aligned}
&= \frac{e^2}{LT}\int_{x,y,z} \hat{H}^{x(\beta)}_D \mathrm{i}D^{zy}_{\mu\nu}\gamma^0_{\alpha\beta}\mathrm{i}G^{xy}_{\beta\kappa}\gamma^\mu_{\kappa\lambda}\mathrm{i}G^{yx}_{\lambda\alpha}\gamma^\nu_{\epsilon\delta}\mathrm{i}G^{zz}_{\delta\epsilon} \\
&= \frac{e^2}{LT}\sum_{q_1}\frac{1}{|q_1|^2}\sum_{\substack{k_1,s_1\\ n_1,n_2}} \bar{v}^{k_1s_1}_{\epsilon n_1}\gamma^\mu_{\epsilon\delta}v^{k_1s_1}_{\delta n_2}\delta_{q_1-Q(n_1-n_2)} \\
&\times\left\{\sum_{\substack{k_1,p_1\\ s_1,s_2}} \frac{\sum_{n_1,n_2}\bar{u}^{k_1s_1}_{\kappa n_1}\gamma^\mu_{\kappa\lambda}v^{p_1s_2}_{\lambda n_2}\delta_{p_{n_2}+k_{n_1}-q_1}\sum_{n_1,n_2}\bar{v}^{p_1s_2}_{\alpha n_1}\gamma^0_{\alpha\beta}u^{k_1s_1}_{\beta n_2}\epsilon^{(+)}_{k_1s_1}\delta_{p_{n_1}+k_{n_2}}}{\epsilon^{(-)}_{p_1s_2}+\epsilon^{(+)}_{k_1s_1}}\right. \\
&\left.-\sum_{\substack{k_1,p_1\\ s_1,s_2}} \frac{\sum_{n_1,n_2}\bar{v}^{k_1s_1}_{\kappa n_1}\gamma^\mu_{\kappa\lambda}u^{p_1s_2}_{\lambda n_2}\delta_{p_{n_2}+k_{n_1}+q_1}\sum_{n_1,n_2}\bar{u}^{p_1s_2}_{\alpha n_1}\gamma^0_{\alpha\beta}v^{k_1s_1}_{\beta n_2}\epsilon^{(-)}_{k_1s_1}\delta_{p_{n_1}+k_{n_2}}}{\epsilon^{(+)}_{p_1s_2}+\epsilon^{(-)}_{k_1s_1}}\right\}.
\end{aligned} \tag{C21}$$

The exchange diagrams are given as

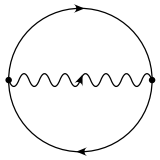
$$\begin{aligned}
&= \frac{\mathrm{i}e^2}{LT}\gamma^\nu_{\alpha\beta}\gamma^\mu_{\kappa\lambda}\int dx\int dy \mathrm{i}G^{\beta\kappa}_{xy}\mathrm{i}G^{\lambda\alpha}_{yx}\mathrm{i}D^{\mu\nu}_{yx} \\
&= \frac{e^2}{2LT}\sum_{\substack{k_1p_1q_1\\ s_1s_2}}\sum_{\substack{n_1n_2\\ n_3n_4}}\left[\frac{\bar{v}^{p_1s_2}_{\alpha n_4}\gamma^\mu_{\alpha\beta}u^{k_1s_1}_{\beta n_1}\delta_{k_{1,n_1}+p_{1,n_4}+q_1}\bar{u}^{k_1s_1}_{\kappa n_2}\gamma^\mu_{\kappa\lambda}v^{p_1s_2}_{\lambda n_3}\delta_{k_{1,n_2}+p_{1,n_3}+q_1}}{|q_1|(|q_1|+\epsilon^{(+)}_{k_1s_1}+\epsilon^{(-)}_{p_1s_2})}\right.
\end{aligned}$$

$$+\frac{\bar{u}^{p_1s_2}_{\alpha n_4}\gamma^{\mu}_{\alpha\beta}v^{k_1s_1}_{\beta n_1}\delta_{k_{1,n_1}+p_{1,n_4}-q_1}\bar{v}^{k_1s_1}_{\kappa n_2}\gamma_{\mu\kappa\lambda}u^{p_1s_2}_{\lambda n_3}\delta_{k_{1,n_2}+p_{1,n_3}-q_1}}{|q_1|(|q_1|+\epsilon^{(-)}_{k_1s_1}+\epsilon^{(+)}_{p_1s_2})}\Bigg], \tag{C22}$$

and

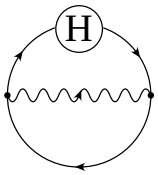

$$= -\frac{e^2}{2LT}\int_{x,y,z}\gamma^0_{\alpha\beta}\gamma^{\mu}_{\epsilon\delta}\gamma^{\nu}_{\kappa\lambda}\hat{H}^{(\beta)}_{D,x}(\bar{A})(\mathrm{i}D^{\mu\nu}_{yz}\mathrm{i}G^{\lambda\epsilon}_{zy}\mathrm{i}G^{\beta\kappa}_{xz}\mathrm{i}G^{\delta\alpha}_{yx})$$

$$= \frac{e^2}{4LT}\sum_{\substack{k_1p_1r_1q_1\\ s_1s_2s_3}}\frac{1}{|q_1|}$$

$$\Big[\frac{\sum_{n_1n_2}\bar{u}^{k_1s_1}_{n_1}\gamma_{\mu}v^{r_1s_3}_{n_2}\delta_{k_{1,n_1}+r_{1,n_2}+q_1}\sum_{n_1n_2}\bar{u}^{p_1s_2}_{n_1}\gamma^{\mu}u^{k_1s_1}_{n_2}\delta_{k_{1,n_2}-p_{1,n_1}+q_1}}{(|q_1|+\epsilon^{(+)}_{k_1s_1}+\epsilon^{(-)}_{r_1s_3})(\epsilon^{(+)}_{p_1s_2}+\epsilon^{(-)}_{r_1s_3})}$$

$$\sum_{n_1n_2}\bar{v}^{r_1s_3}_{n_1}\gamma^0u^{p_1s_2}_{n_2}[\epsilon^{(+)}_{p_1s_2}\delta_{p_{1,n_2}+r_{1,n_1}}]+$$

$$\frac{\sum_{n_1n_2}\bar{u}^{k_1s_1}_{n_1}\gamma_{\mu}u^{r_1s_3}_{n_2}\delta_{k_{1,n_1}-r_{1,n_2}+q_1}\sum_{n_1n_2}\bar{v}^{p_1s_2}_{n_1}\gamma^{\mu}u^{k_1s_1}_{n_2}\delta_{k_{1,n_2}+p_{1,n_1}+q_1}}{(|q_1|+\epsilon^{(+)}_{k_1s_1}+\epsilon^{(-)}_{p_1s_2})(\epsilon^{(-)}_{p_1s_2}+\epsilon^{(+)}_{r_1s_3})}$$

$$\sum_{n_1n_2}\bar{u}^{r_1s_3}_{n_1}\gamma^0v^{p_1s_2}_{n_2}[-\epsilon^{(-)}_{p_1s_2}\delta_{p_{1,n_2}+r_{1,n_1}}]-$$

$$\frac{\sum_{n_1n_2}\bar{u}^{k_1s_1}_{n_1}\gamma_{\mu}v^{r_1s_3}_{n_2}\delta_{k_{1,n_1}+r_{1,n_2}+q_1}\sum_{n_1n_2}\bar{v}^{p_1s_2}_{n_1}\gamma^{\mu}u^{k_1s_1}_{n_2}\delta_{k_{1,n_2}+p_{1,n_1}+q_1}}{(|q_1|+\epsilon^{(+)}_{k_1s_1}+\epsilon^{(-)}_{p_1s_2})(|q_1|+\epsilon^{(+)}_{k_1s_1}+\epsilon^{(-)}_{r_1s_3})}$$

$$\sum_{n_1n_2}\bar{v}^{r_1s_3}_{n_1}\gamma^0v^{p_1s_2}_{n_2}[-\epsilon^{(-)}_{p_1s_2}\delta_{p_{1,n_2}-r_{1,n_1}}]+$$

$$\frac{\sum_{n_1n_2}\bar{v}^{k_1s_1}_{n_1}\gamma_{\mu}u^{r_1s_3}_{n_2}\delta_{k_{1,n_1}+r_{1,n_2}-q_1}\sum_{n_1n_2}\bar{u}^{p_1s_2}_{n_1}\gamma^{\mu}v^{k_1s_1}_{n_2}\delta_{k_{1,n_2}+p_{1,n_1}-q_1}}{(|q_1|+\epsilon^{(-)}_{k_1s_1}+\epsilon^{(+)}_{p_1s_2})(|q_1|+\epsilon^{(-)}_{k_1s_1}+\epsilon^{(+)}_{r_1s_3})}$$

$$\sum_{n_1n_2}\bar{u}^{r_1s_3}_{n_1}\gamma^0u^{p_1s_2}_{n_2}[\epsilon^{(+)}_{p_1s_2}\delta_{p_{1,n_2}-r_{1,n_1}}]-$$

$$\frac{\sum_{n_1n_2}\bar{v}^{k_1s_1}_{n_1}\gamma_{\mu}u^{r_1s_3}_{n_2}\delta_{k_{1,n_1}+r_{1,n_2}-q_1}\sum_{n_1n_2}\bar{v}^{p_1s_2}_{n_1}\gamma^{\mu}v^{k_1s_1}_{n_2}\delta_{k_{1,n_2}-p_{1,n_1}-q_1}}{(|q_1|+\epsilon^{(-)}_{k_1s_1}+\epsilon^{(+)}_{r_1s_3})(\epsilon^{(-)}_{p_1s_2}+\epsilon^{(+)}_{r_1s_3})}$$

$$\sum_{n_1n_2}\bar{u}^{r_1s_3}_{n_1}\gamma^0v^{p_1s_2}_{n_2}[-\epsilon^{(-)}_{p_1s_2}\delta_{p_{1,n_2}+r_{1,n_1}}]-$$

$$\frac{\sum_{n_1n_2}\bar{v}^{k_1s_1}_{n_1}\gamma_{\mu}v^{r_1s_3}_{n_2}\delta_{k_{1,n_1}-r_{1,n_2}-q_1}\sum_{n_1n_2}\bar{u}^{p_1s_2}_{n_1}\gamma^{\mu}v^{k_1s_1}_{n_2}\delta_{k_{1,n_2}+p_{1,n_1}-q_1}}{(|q_1|+\epsilon^{(-)}_{k_1s_1}+\epsilon^{(+)}_{p_1s_2})(\epsilon^{(+)}_{p_1s_2}+\epsilon^{(-)}_{r_1s_3})}$$

$$\sum_{n_1n_2}\bar{v}^{r_1s_3}_{n_1}\gamma^0u^{p_1s_2}_{n_2}[\epsilon^{(+)}_{p_1s_2}\delta_{p_{1,n_2}+r_{1,n_1}}]\Big]. \tag{C23}$$

5. Numerical procedure

The one-particle energy levels and spinors needed for the calculation were determined by solving numerically the system of linear equations (A4) and the sum over the components of the Bloch-waves was truncated for $|n| \leq 25$. This procedure provided us 50 one-particle energy levels and spinors for each momentum in the first Brillouin zone. It was tested on the fermion spectrum without background field that such a truncation starts to cause noticeable error on the spectrum for the band index $s \approx n$ when the bands are numerated in energetically increasing order. Therefore, bands

with $s \leq 20$ have been taken into account in the calculations of the two-loop diagrams. Such a truncation allowed us to detect the effects of the background field with sufficient accuracy because it was found that for $ea \leq m$ the distortion of the dispersion relation due to the background field is only significant for states belonging to the bands in the vicinity of m. For about 5 bands away from m the deviation of the energy levels with and without the periodic background field turns practically to zero. The one- and two-loop diagrams of Eq. (41) were computed in the first Brillouin zone $k_1 \in [-Q/2, Q/2)$ at 40 and 10 points, respectively. The calculation of the one-loop diagram required higher numerical accuracy due to the numerical elimination of the UV divergence. We also made a test calculation for 20 division points which corresponded to a larger volume L and found that the numerical accuracy is about 10% for the two-loop contribution to the Casimir-energy density in the whole range of the parameter values.

The amplitude a was chosen through several orders of magnitude from $ea = 10^{-4}$ corresponding to the perturbative regime to $ae \approx m$ for which pair-production might occur. The wavenumber of the background field was restricted to be $Q = 0.8, 1, 1.5$ in the computation. The significantly smaller values are uninteresting from the point of view of the periodic state since the electrons become well localized in the limit $1/Q \to \infty$ and it would cost too much energy to delocalize them. The other limit $1/Q \to 0$ is computationally time-consuming since one has to take more Brillouin-zones into account. Therefore the summations over the band index s, as well as over the one-particle state's index n have to be truncated at increasingly higher values in the formulae of App. C 1. Consequences of this very restricted search of the minimum of the Casimir-energy density not allowing for the higher values $Q > 1.5$ make our numerical results unreliable for large densities. The calculations were performed on an AlphaServer DS20 500 MHz with 2 CPU-s. In particular, it took about 2 CPU hours on a single processor to compute the diagrams in Eq. (41) for a given set of parameters $(ea, e\mu/m, m)$ for $Q = 0.8$. For any given set of (Q, ea, m) we chose 50 values for $0.5 \leq e\mu/m \leq 2$ in such a manner that the points between 0.98 and 1.35 were separated by 0.01. For $m = 1$ we took $a = 0.0001, 0.001, 0.01, 0.1, 0.2, 0.5, 1.0$ and $Q = 0.8, 1.0, 1.5$. For $m = 0.2, 0.5, 2.0$ and 5.0 we took only the 4 larger values of a.

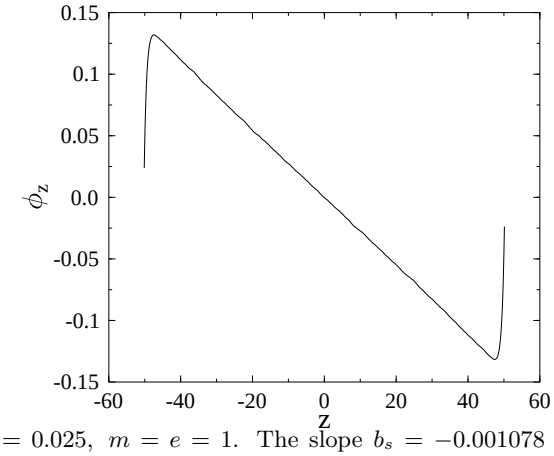

FIG. 1. The scalar field ϕ_z for $b = 0.025,\ m = e = 1$. The slope $b_s = -0.001078$ fitted in the central region should be compared to $b_s = be^2/(\kappa^2\pi) = -0.001074$ from Eq. (19).

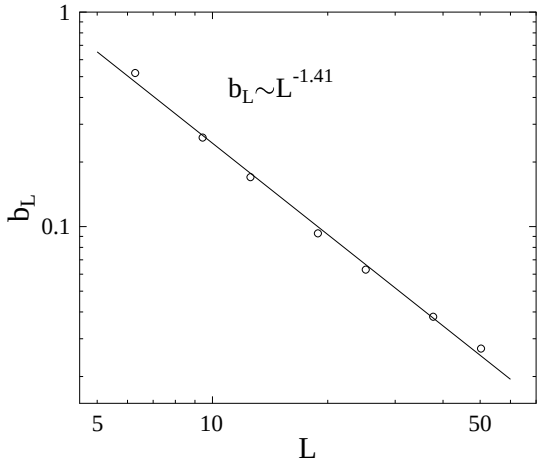

FIG. 2. Dependence of the point $b_{\rm L}$ on the size L of the system for $m = e = 1$.

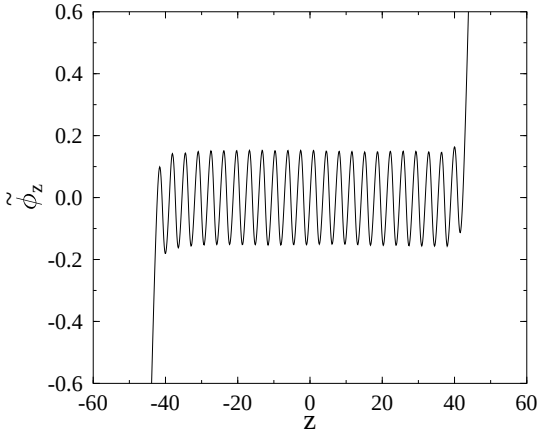

FIG. 3. The periodic part $\tilde{\phi}_z$ of the scalar ground-state field configuration for $b = 0.5, m = e = 1$.

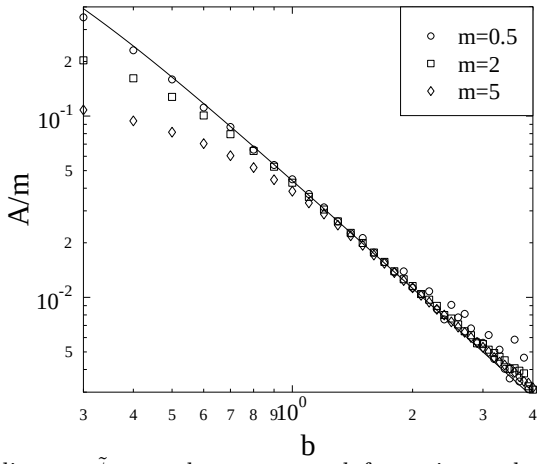

FIG. 4. Amplitude A of the periodic part $\tilde{\phi}_z$ vs. the parameter b for various values of the electron mass m and $e = 1$. The solid line represents our perturbative estimate for the amplitude given by Eq. (24). The numerical values justify the perturbative estimate for small values of A.

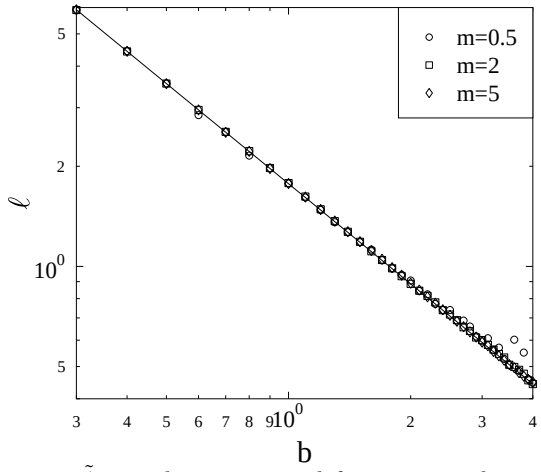

FIG. 5. Wavelength ℓ of the periodic part $\tilde{\phi}_z$ vs. the parameter b for various values of the electron mass m and $e = 1$. The solid line refers to the curve $\ell = \sqrt{\pi}/b \equiv 1/\rho_{\rm ext}$.

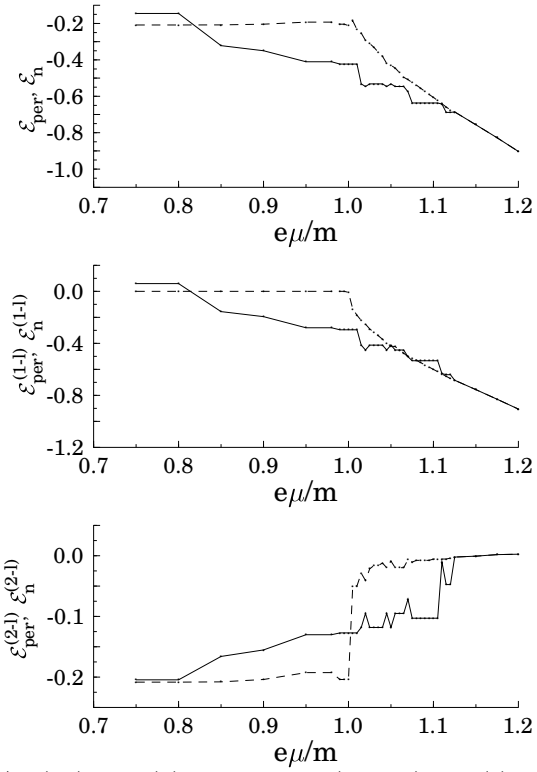

FIG. 6. (a) Energy densities vs. $e\mu/m$ (up), and (b) the one-loop (middle) and (c) two-loop (down) contributions to those. The solid and dashed lines refer to the periodic and the homogeneous phases, respectively.

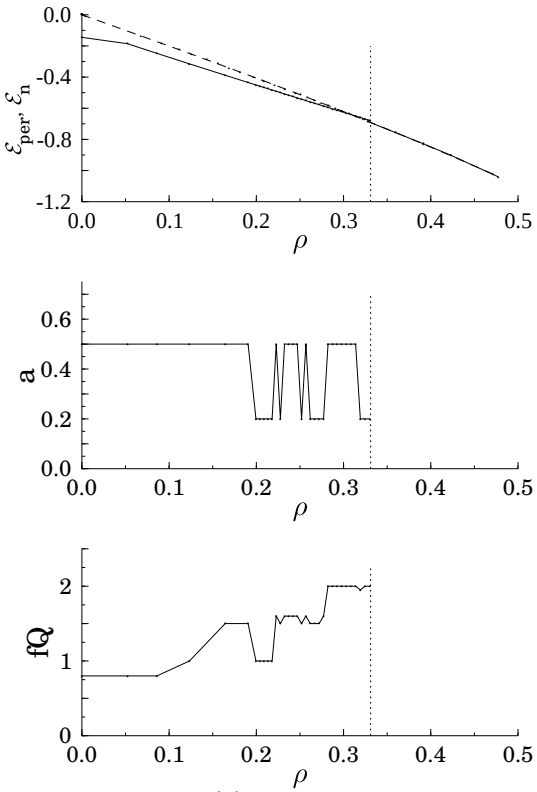

FIG. 7. Density dependences of (a) the energy density, (b) the amplitude a of the photon condensate and (c) the product of the filling factor f and the wavenumber Q of the photon condensate for $m = 2$. The dotted lines indicate the 'critical charge density' ρ_c, solid and dashed lines correspond to the periodic and normal phases, respectively.

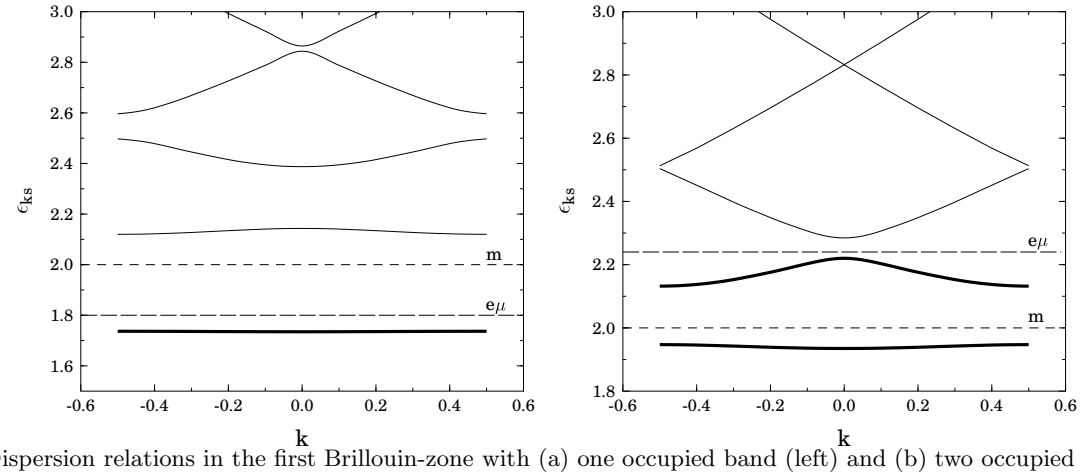

FIG. 8. Dispersion relations in the first Brillouin-zone with (a) one occupied band (left) and (b) two occupied bands (right) sunk into the Dirac sea for $ea = 0.5$ and $ea = 0.2$, respectively, $m = 2$.

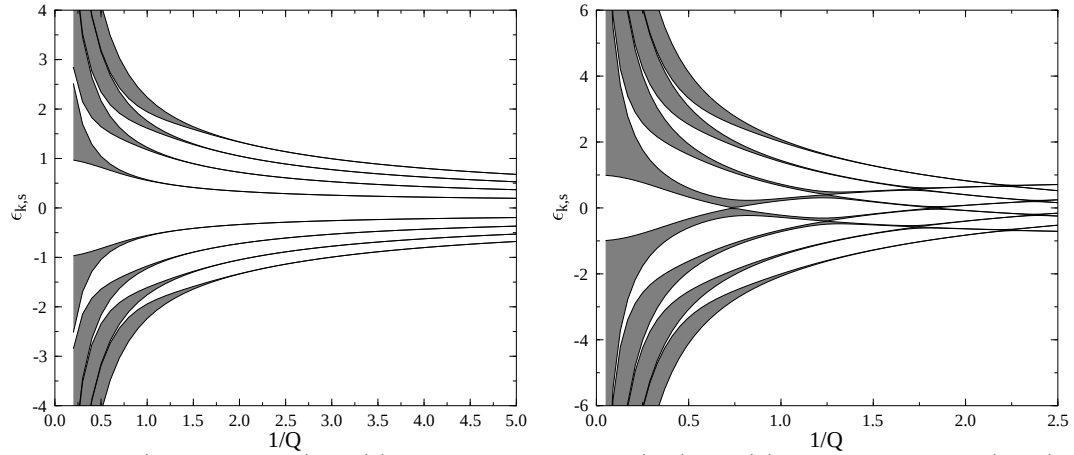

FIG. 9. Allowed bands (shaded regions) for (a) undercritical $ea = 0.9$ (left) and (b) overcritical $ea = 2$ (right) static periodic external fields with wavenumber Q for $m = e = 1$.

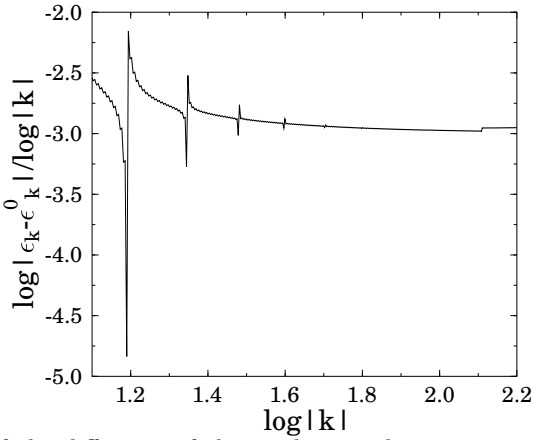

FIG. 10. Momentum-dependence of the difference of the single particle energies in the expression (C16) of the one-loop energy for $m = 2$, $Q = 1.1$ and $a = 2$.